Norbert Csongovai

Discrete modelling of the dual active bridge converter

Master thesis
Norwegian University of Science and Technology
Faculty of Information Technology and Electrical Engineering
Department of Electric Power Engineering
June 2022

NTNU

Table of Contents

1 Introduction **8**
1.1 The outline of the thesis 9

2 Chapter 2 - Generic DAB converter features **10**
2.1 DAB converter characteristics under SPS modulation 14
2.2 DAB converter characteristics under EPS modulation 16

3 Chapter 3 - Discrete modelling and control of the DAB converter **19**
3.1 State space modelling 19
3.2 Considerations on the nonlinearity of SPCs 22
3.3 Derivation of the DAB converter model 28
3.3.1 The simple model of a Buck converter 30
3.3.2 The discrete time model under SPS modulation 39
3.3.3 The DAB converter model under EPS modulation 49

4 Chapter 4 - Numerical example and discussion **55**
4.1 Validating the model of the Buck converter 55
4.2 Validating the model of the DAB converter 59
4.3 Discussions 63

Bibliography **65**

List of Figures

1 A dual active bridge (DAB) converter 9

2 Si and SiC main physical parameters, from [2] 10

3 Comparison of main physical characteristics of Si, 4H-SiC and 2H-GaN, from [3] 11

4 Important physical parameters of Si, SiC and GaN, from [4] 11

5 Characteristics of a choice of magnetic materials, from [5] 12

6 The simple equivalent circuit of a DAB converter 13

7 DAB converter operation under SPS modulation 14

8 DAB converter waveforms under EPS modulation 17

9 The bifurcation diagram of the logistic equation 23

10 PWM diagram, from [15] 27

11 DAB converter diagram representing the first 28

12 DAB converter diagram representing the second state 28

13 DAB converter diagram representing the third state 29

14 DAB converter diagram representing the fourth state 29

15 The Buck equivalent model of the DAB converter in states 2 and 3 29

16 the Buck converter 30

17 Buck converter circuit diagram in the OFF state 32

18 2 gains feedback loop for pole placement 36

19 Single gain version of the pole placement method 37

20 The simplified diagram of a DAB converter, ignoring R_t andR_c 39

21 The DAB converter, including R_t and R_c 40

22 DAB converter in the 2^{nd} state 42

23 DAB converter circuit diagram representing the first state 49

24 DAB converter circuit diagram representing the second state 51
25 DAB converter circuit diagram representing the third state 51
26 DAB converter circuit diagram representing the fourth state 51
27 DAB converter circuit diagram representing the fifth state 53
28 DAB converter circuit diagram representing the sixth state 53
31 Buck converter bifurcation diagram 57
33 the inductor current of the DAB converter under SPS 59
34 close caption of the waveform of the inductor current under SPS 60
35 the capacitor voltage of the DAB converter under SPS 60
36 close caption of the waveform of the capacitor voltage under SPS 61
37 the inductor current of the DAB converter under EPS 61
38 close caption of the inductor current under EPS 62
39 the capacitor voltage of the DAB converter under EPS 62
40 close caption of the capacitor voltage under EPS 63

Abstract

The importance of the bidirectional DC-to-DC power converters cannot be exaggerated in the context of today's power grids. As distributed energy resources become an integral part of electrical energy infrastructure, the ability to send power bidirectionally between source and load provides increased quality and flexibility to the power infrastructure as a whole, and the concept of smart grids in particular. The dual active bridge (DAB) DC-to-DC converter has therefore been in the centre of attention due to its advantages over other devices of similar abilities, but it does not come without flaws and challenges. The purpose of this paper is to focus on one of these challenges, namely finding an optimal modelling technique for the converter.

This thesis recounts the main characteristics of the DAB converters, listing both its positive and negative attributes. By the means of literature review, state space modelling, and simulation, the nonlinear nature of the converter is explored, and a suitable modelling technique is presented. The main goal of the present work is to serve as extensive and sufficient support for future work, aimed at developing and implementing a modern, optimal control technique for the DAB converter.

The main contribution of this thesis is the detailed derivation of a discrete time model for the DAB converter, considering its operation both under single phase shift (SPS) and extended phase shift (EPS) modulation. With the purpose of developing the intuition of the reader, the relatively simple example of a Buck converter is covered as well. The nonlinear traits of the DAB converter are demonstrated by performing elementary stability analysis. The model is then tested and the relevant results are presented.

Sammendrag

Bidirekskjonelle DC-til-DC omformere spiller en meget viktig rolle i dagens elektriske energi infrastruktur. Ettersom distribuerte ressurser har blitt en aktiv del av elnettverket, evnen til å sende kraft til-og fra last muliggjør en mer effektiv og fkeksibel utnyttelse av infrastrukturen i sin helhet, og hovedsakelig av smartgrid konseptet. På grunn av sine mange fordeler sammenlignet med andre omformer-konfigurasjoner, har den "dual active bridge" (DAB) likespenning - til - likespenning omformeren fått stadig økende oppmerksomhet. Den har dog sine ulemper og utfordringer. Det er en av disse utfordringene som denne masteroppgaven setter fokuset på, i form av å fremlegge en velfungerende matematisk model av omformeren.

Avhandlingen studerer og presenterer hovedegenskapene til DAB omformeren, både de postitive, så vel som de negative. Gjennom literaturstudie, tidsromanalyse, og simulering er omformerens ikke-ineare egenskapene belyst. Videre, det presenteres gjennomgangen av en velegnet model, som tar høyde for de ikke-lineare egenskapene til DAB omformeren. Avhandlingens hovedmål er at den skal kunne brukes som fullverdig og tilstrekkelig støttemateriell i fremtidige forsøk på å utvikle, og å implementere en moderne reguleringsmekanisme for DAB omformeren.

Masteroppgavens hovedbidrag er en grunndig undersøkelse av en diskret model for DAB omformeren, som belyser omformerens drift når den blir regulert ved hejlp av enkel faseforskyvning, så vel som forlenget faseforskyvning. Med tanke på å utvikle intuisjon og forståelse for temaet, den diskrete modelen er i tillegg tilpasset en Buck omfomer, som har en mindre komplisert struktur enn DAB omformeren. De ikke-lineare egenskapene til DAB omformeren er belyst ved hjelp av enkel stabilitetsanalyse. Modelen er til slutt validert, og de relevante resultater lagt frem.

Preface

This master's thesis completes my MSc degree in Energy and Environmental Engineering at the Norwegian University of Science and Technology (NTNU). It has been carried out at the Department of Electric Power Engineering during the spring semester of 2022. The thesis builds on my specialisation project conducted in the autumn semester of 2021, whose objective was to be thoroughly acquainted with the structure, components, operating mechanism, and phase shift modulation techniques of the dual active bridge (DAB) converter. This thesis investigates a discrete time model of the DAB converter, that is designed to match the nonlinear nature of the converter.

I would hereby like to thank my supervisor Professor Dimosthenis Peftitsis, for his assistance and for granting me the possibility of writing this paper. I would also like to express my gratitude to my co-supervisor, PhD candidate Yoganandam Vivekanandham Pushpalatha who has provided me with invaluable input and assistance, for always being available for discussion and enabling me to gain understanding and vanquish confusion. I am also grateful to the other wonderful professors and academic support staff that I have had the privilege of asking for guidance during these past years.

These past five years have given me more than mere theoretical knowledge related to power engineering. NTNU has given me the possibility to grow as a person, to develop new ways of understanding the outside world. I have been reminded of the beauty of studying, the pleasure that comes with learning new skills, or grasping a new concept that seemed daunting in the beginning. I am truly grateful.

1 Introduction

The train of thought is relatively simple: as the population of the planet increases, the need for energy is increasing as well. This need can be addressed by several types of energy exploitation. But as the planet's population has become aware of the negative repercussions of burning fossil fuels to obtain the necessary energy, considerable efforts are being made to transition towards renewable energy sources. It is both in the interest of industrialised nations, as well as poor countries, to embrace the more efficient and environmentally friendly energy sources. In the matter of different forms of useful energy, electrical energy is far superior to the other forms, as it allows for near lossless transformation between electrical and mechanical energy, and thus delivering higher efficiency, than for example heat energy is able to do.

The area of power electronics has been subjected to accelerated developments the last few decades. As electrification was becoming an important issue, the flaws of and shortcomings of the infrastructure have become increasingly evident. Just as constructing new highways is a costly affair, both money-wise and from a spatial point of view, maintaining and developing the electrical energy infrastructure must be subjected to careful planning and assessment. With the help of power electronic devices we are able to upgrade and improve the existing infrastructure, as well as find ingenious ways of designing the future components.

The power grids of the future, rightfully referred to as smart grids, are to be fully digitalised. This allows for establishing better channels of communication and control, enabling new characteristics that the traditional power networks are not capable of providing. Distributed energy resources (DER) will be a structural part of the future energy infrastructures. Power electronic devices are a crucial components of the smart grid. Switchable DC-to-DC converters have proven their worth, in applications ranging from the smallest scale of a regular household appliance, to huge offshore power transmission platforms.

One such device is the dual active bridge (DAB) converter. The virtues of the DAB converter are originating from its architecture, as well as its components. A diagram of a generic DAB converter is depicted in figure 1.

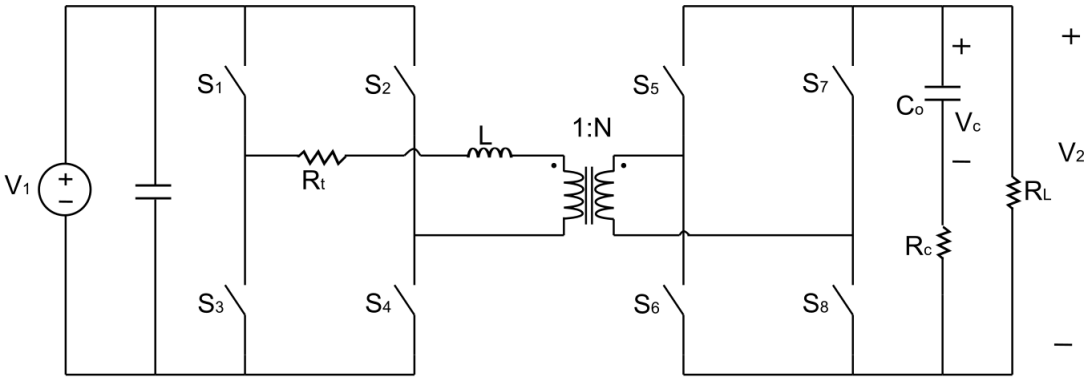

Figure 1: A dual active bridge (DAB) converter

It is made up of two full bridges equipped with switches, like in the form of SiC MOSFETs, a high frequency transformer (HFT), and an output filter capacitor. It is a DC-to-DC converter that provides bi-directional power flow, and thus can either operate as a buck or boost converter. Its main advantages lie in the galvanic isolation obtained with the help of the HFT, and considerable reduction of the physical volume. Due to its low number of components it is relatively robust, and provided the switching frequency is kept at a reasonably high level, the converter can also be run quite efficiently, exhibiting efficiency measurements in excess of 96%.

1.1 The outline of the thesis

This paper focuses on the discrete modelling and control of the dual active bridge (DAB) converter in the context of instability caused by the inherent nonlinear nature of switched power electronic devices. The build-up to this master thesis was a specialisation project that I have conducted in the form of a literature review in the previous semester. This review took a thorough look at the general properties of a SiC MOSFET equipped DAB converter. The steady-state characteristics of the converter have been derived and simulated in PLECS - a software tool for simulation electrical systems.

The main findings of this review will be presented in this paper in **chapter 2**, so that the reader is made familiar with the subject of this thesis.

Following this simple introductory chapter, a discrete model and proportional control of the DAB converter are presented in detail in **chapter 3**.

In **chapter 4** the theory of the previous chapter is validated. The discrete model and controller are observed by running a series of simulations using numerical values. The nonlinear behaviour of the DAB converter is tested by means of elementary stability analysis. This final chapter is then concluded by discussing the relevant findings, and describing the remaining tasks that are based on this thesis.

2 Chapter 2 - Generic DAB converter features

The DAB converter depicted in figure 1 is symmetrical in its structure. The main advantages of this converter type have been known for several decades now[1]:

- small number of components
- low device and component stress
- zero (or low) switching losses under zero voltage, - and zero current switching (ZVS and ZCS respectively)
- small filter components
- high efficiency (no trapped energy)
- bi-directional power flow, implying that buck operation is possible with the power flowing in one direction, while reversing the direction of the power flow would enable boost operation
- low sensitivity to system parasitics
- parallel operation possible

It has four MOSFET switches on the primary side and four on the secondary side. The current will always be conducted by a cross-diagonal pair of switches, or their corresponding Schottky diodes. The choice of components is important relative to maximising the power transmission. Due to a number of superior characteristics, summarised below, it is preferred to equip the DAB converter with SiC MOSFETs, as opposed to the more commonplace SI devices.

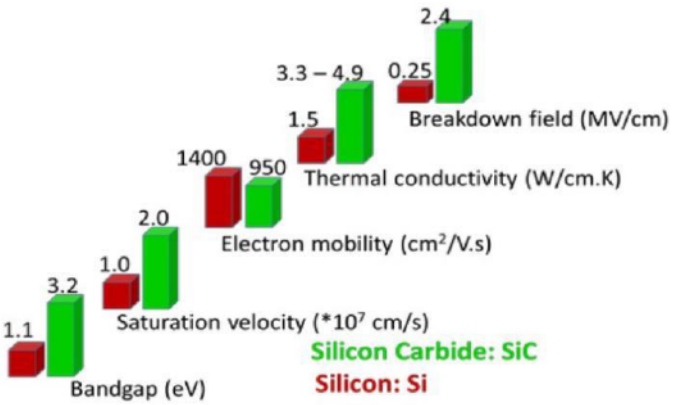

Figure 2: Si and SiC main physical parameters, from [2]

GaN is another viable alternative to the mature Si devices. The characteristics of gallium nitrate are comparable to SiC, even superior in some aspects, as shown below:

property	Si	4H-SiC	2H-GaN
bandgap (eV)	1.12	3.2	3.4
critical field E_{cr} (MV cm^{-1})	0.25	3	4
electron mobility μ (cm^{2}V^{-1} s^{-1}) (2DEG)	1350	800	1300
saturation velocity v_s (10^7 cm s^{-1})	1	2	3
thermal conductivity k (W cm^{-1}K^{-1})	1.5	4.9	1.3
intrinsic carrier concentration n_i (cm^{-3}) at 300 K	10^{10}	10^{-7}	10^{-10}
dielectric constant ε	11.8	9.7	9.5
JFOM $(v_sE_{cr})^2/(v_sE_{cr})^2$Si	1	576	2304
BFOM $(\varepsilon\mu E_{cr}^3)/(\varepsilon\mu E_{cr}^3)$Si	1	842	3175
BHFOM $(\mu E_{cr}^2)/(\mu E_{cr}^2)$Si	1	85	246

Figure 3: Comparison of main physical characteristics of Si, 4H-SiC and 2H-GaN, from [3]

and in:

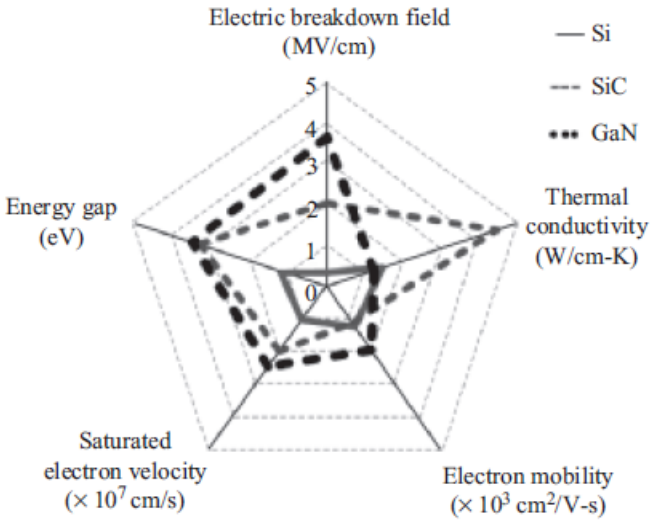

Figure 4: Important physical parameters of Si, SiC and GaN, from [4]

The other main component of the DAB converter is the HFT. There are mainly three types of materials that exhibit notable characteristics:

- amorphous materials present high magnetic saturation abilities, but at the cost of rather significant specific losses
- ferrite materials have poor magnetic saturation values, but present very low specific losses
- nano crystalline materials appear to be a good compromise between the two types mentioned above, possessing both high magnetic saturation threshold, and low specific loss values

The following table is presenting numeric values to aid the reader in constructing a general idea of the available materials and their most important characteristics:

Magnetic Material Type	Material	Manuf.	B_{sat}	Specific Losses @ 0.1 T, 100 kHz	Continous Operating Temperature
Sil.Steel	10JNHF600	JFE [95]	1.87 T	0.24 kW/kg	150°C
Sil.Steel	10NEX900	JFE	1.6 T	0.19 kW/kg	150°C
Amorphous	2605SA1	Metglas [96]	1.56 T	0.2 kW/kg	150°C
Ferrite	3C85 [97]	Ferroxcube	0.45 T	0.009 kW/kg	140°C
Ferrite	3C93	Ferroxcube	0.52 T	0.009 kW/kg	140°C
Powder	Xflux 60	Magnetics [98]	1.6 T	0.26 kW/kg	200°C
Powder	KoolMu 125	Magnetics	1.05 T	0.14 kW/kg	200°C
Nano.Crys	Vitroperm500F	VAC [99]	1.2 T	0.01 kW/kg	120°C
Nano.Crys	Finement	Hitachi [100]	1.23 T	0.011 kW/kg	120°C

Figure 5: Characteristics of a choice of magnetic materials, from [5]

Choosing the optimal components of the converter does not guarantee high efficiency by itself. It is the way that these components are made to interact with each other, that determines the efficiency of the device. There are indeed many control techniques that can be used to operate the DAB converter. Phase shift modulation is relatively easy to comprehend and implement. In its essence, it resumes to controlling the amplitude and direction of the transmitted power, merely by adjusting the phase shift inside the converter. There are four types of phase shift modulation techniques:

1. SPS stands for single phase shift, and it refers to a phase shift between the primary and secondary bridge (it is up to the individual to designate the primary and secondary appellatives)

2. EPS means extended phase shift, and in this case, in addition to the phase shift between the primary and secondary bridges, we also have an internal phase shift in the primary bridge, between the two bridge legs

3. DPS stands for double phase shift, and in this case we have the original phase shift between the primary and secondary bridges, as well as internal phase shifts of equal values between the two bridge legs in both bridges

4. the fourth technique is the triple phase shift, TPS, where we have the same setup as in the DPS, but this time the values of the internal phase shifts of the two bridges are no longer identical

One of the most common problems in the industry is poorly tuned converters, resulting in poor efficiency. It is then fortunate that in the case of the DAB converter the simplest modulation technique allows for the highest power transfer between the primary and secondary bridges: SPS, run with a 50 % duty ratio. The maximum power transmission does however come at the cost of some loss, in the form of backflow power. This loss can be minimised by using EPS modulation, with the downside of not being able to transmit the same amount of power as in SPS.

For understanding the conceptual operation of the DAB converter, both under SPS and EPS modulation techniques, a simple circuit diagram of a DAB converter equivalent is employed. Given that the DAB is made up of 2 H-bridges, equipped with four switches each, it can be noted that that one switch of either leg will be on at any one time, for half a period. As both switches of a given bridge leg are not turned on simultaneously, the output of this bridge is a square wave, constantly shifting between V_1 and -V_1. This constitutes in practice an AC waveform. This AC waveform is passed on to the high frequency transformer, and transmitted to the secondary H-bridge. This HFT can be depicted by its leakage impedance. The operation of this secondary bridge is similar to the first one, but the opposite effect is achieved: the square wave is now rectified, allowing for the output of a DC voltage. This operation, combined with the assumption that the HFT and the switches are all ideal components, is effectively captured by the diagram depicted below in figure 6:

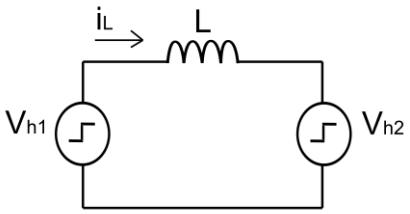

Figure 6: The simple equivalent circuit of a DAB converter

However, for clearly understanding the states that the converter goes through during one switching cycle, it is best to make use of the full converter diagram, as it is done in the subsequent sections of this paper.

2.1 DAB converter characteristics under SPS modulation

The derivation of the main characteristics of the DAB converter under SPS modulation are based on figure 7.

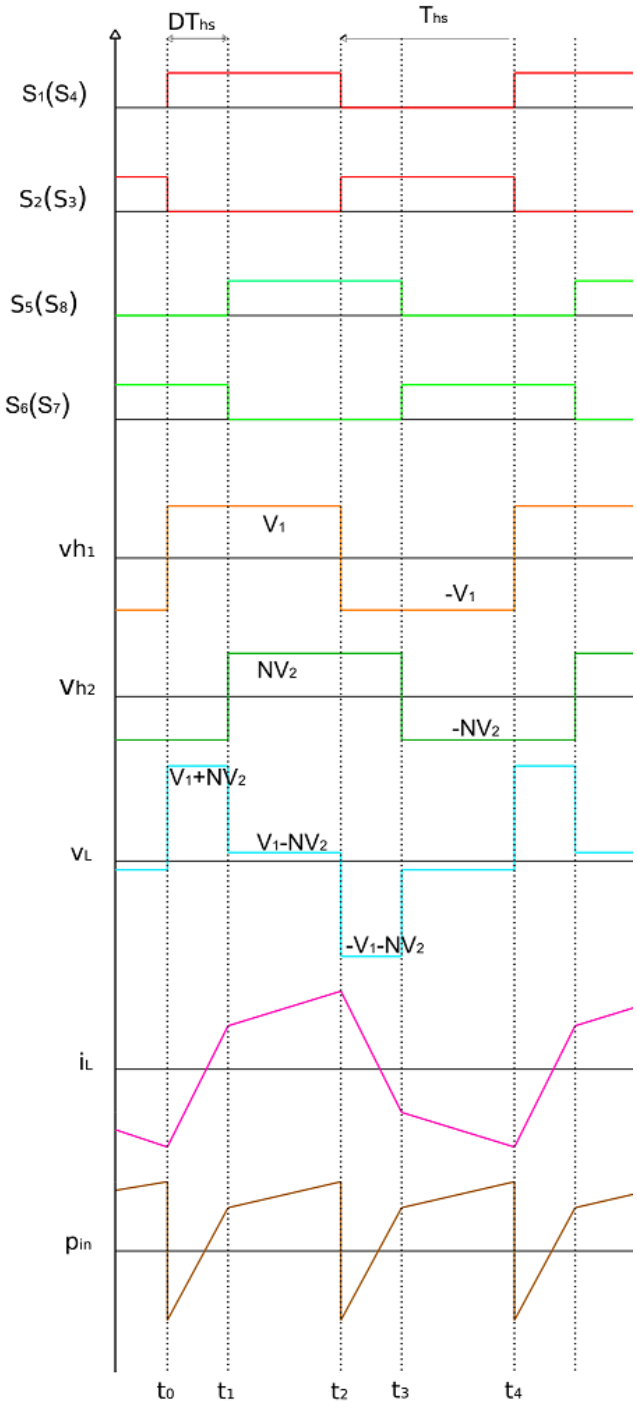

Figure 7: DAB converter operation under SPS modulation

The equations defining the magnitude of the inductor current for each of the four time instants, from t_0 to t_4 have been derived in my specialisation project that this paper is based upon [6]. These equations yielded the expression for the power transfer under SPS:

$$P_{SPS} = \frac{NV_1V_2}{2f_sL} \cdot D(1-D) \tag{1}$$

where:

- N is the windings ratio of the HFT
- V_1 is the input voltage to the primary, high voltage side, and the notations V_1 and V_p are used interchangeably
- V_2 is the output voltage from the secondary bridge, the low voltage side; this is the voltage seen by the load
- f_s is the switching frequency
- L is the leakage inductance
- D is the phase shift between the primary and secondary bridges

There is, however, another power parameter, just as relevant as the transmitted power, and this is the reflow power - which is lost under one switching cycle. Geometrically, the reflow power is visible as the area under the 0 line of the p_{in} parameter, and it can be expressed mathematically as:

$$\begin{aligned} P_{rf,SPS} &= \frac{1}{T_s} \cdot \int_{t_0}^{t_0'} V_1 i_L(t)dt + \int_{t_2}^{t_2'} -V1 i_L(t)dt \Longleftrightarrow \\ P_{rf,SPS} &= \frac{2V1}{T_s} \cdot \int_{t_0}^{t_0'} i_L(t)dt = -NV_1V_2 \cdot \frac{(2D+k-1)^2}{16Lf_s(k+1)} \end{aligned} \tag{2}$$

. where:

- the crossing time t_0' is given as:

$$t_0' = \frac{T_s}{4(k+1)} \cdot (2D+k-1) \tag{3}$$

- T_s is the switching period
- k is the ratio between the input voltage to the primary and the the output voltage of the secondary, adjusted with the windings ratio N:

$$k = \frac{V_1}{NV_2} \tag{4}$$

There are several observations to be made. Firstly, both V_2 and k depend on the value of the steady state duty ration D:

$$V_2 = \frac{NV_1R_1}{2f_sL} \cdot D(1-D) \tag{5}$$

For the derivation of the equation of the reflow power, the maximum value of the inductor current is identified as:

$$i_{max} = \frac{NV_2Ts}{4L} \cdot (2D + k - 1) = \frac{NV_2}{4Lf_s} \cdot (2D + k - 1) \tag{6}$$

An important attribute of the SPS modulation scheme worth mentioning is that it enables maximum power transfer in the DAB converter.

2.2 DAB converter characteristics under EPS modulation

Within the subject of phase shift modulation techniques, one should also observe how the system behaves under the extended phase shift modulation. The main advantage of the EPS technique is that the reflow power is reduced due to the extended range of ZVS. The main characteristics of the DAB converter operated under EPS are derived based on figure 8.

The transmitted power is derived by starting with the voltages on the primary and secondary sides. Obtaining the voltage and current over the leakage inductance is next, concluding with the following expression:

$$P = \frac{1}{T_{hs}} \cdot \int_0^{T_{hs}} v_{h1} i_L(t) dt \tag{7}$$

yielding that [7]

$$P_{EPS} = \frac{NV_1V_2}{2f_sL} \cdot (D_2 - D_2^2 + \frac{D_1}{2} - \frac{D_1^2}{2} - D_1D_2) \tag{8}$$

where D_1T_{hs} is the phase shift between the two bridge legs of the high voltage primary, and D_2T_{hs} is the phase shift between the first bridge leg of the primary and the secondary, low voltage bridge.

The voltage of the secondary bridge V_2 is given by the following equation:

$$V_2 = \frac{NV_1R_1}{2f_sL}(D_2 - D_2^2 + \frac{D_1}{2} - \frac{D_1^2}{2} - D_1D_2) \tag{9}$$

As for k, it is identical to the expression pertaining to the SPS modulation, found here 4,

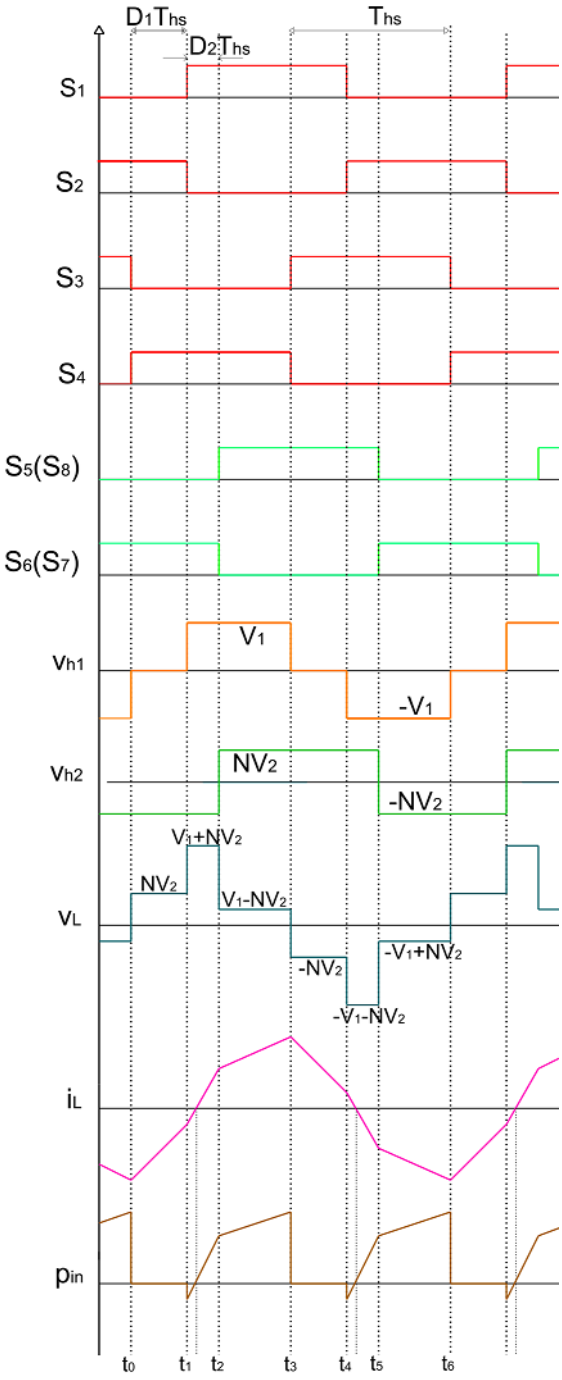

Figure 8: DAB converter waveforms under EPS modulation

repeated below:

$$k = \frac{V_1}{NV_2} \tag{10}$$

The reflow power under EPS is formulated as follows:

$$P_{rf,EPS} = \frac{1}{T_{hs}} \cdot \int_{t_1}^{t_1'} v_{h1}|i_L(t)|dt = \frac{nV_1V_2(k - kD_1 + 2D_2 - 1)^2}{16f_sL(k+1)} \tag{11}$$

and it comes with the following constraints[6]:

- $k \geq 1$
- $0 \leq D_1 \leq 1$
- $0 \leq D_2 \leq 1$
- $0 \leq D_1 + D_2 \leq 1$

As it has been shown in [6], the main advantage of the EPS is a substantial reduction of the reflow power, at the expense of the transmission power. To be more exact, when transferring the exact same amount of power under SPS and EPS modulation, the value of the reflow power will be considerably lower in the case of the EPS, compared to the SPS. Table 1 makes a similar point. Given that no changes are made to the component values of the DAB converter, and by only changing the modulation technique, the converter under EPS will transmit slightly less power, while also reducing the loss in the form of reflow power.

Table 1: SPS and EPS power values

	Transmitted power [kw]	Reflow power [kw]
SPS	100	25
EPS	86.64	16.67
Difference [%]	-13.36	-33

The reduction in reflow power can also be observed by studying figure 8. It is represented by the areas of the small triangles that are formed below the 0 line of p_{in}. Referring to the same figure, it is clear that we now have 6 states describing the voltage over - and current through the inductor over one switching period: from t_0 to t_6. These two additional states in comparison to the DAB converter operated under SPS, are zero voltage states, that yield a longer period of ZVS.

3 Chapter 3 - Discrete modelling and control of the DAB converter

3.1 State space modelling

A DC-to-DC converter will only be useful if it is controllable. Given that there are two different control categories - open loop and closed loop control, one will quickly find that in order to ensure efficiency and stability, the closed loop control is a necessity. A system that does not take into consideration the output in the form of a feedback loop, such a system has no measure of its own efficiency. Simply put, we are always interested in assessing how changes in input parameters affect the values of the output variables.

This relationship between the output and the input, the dependency of the former on the latter, can be contained and expressed by the transfer function. It then follows that in order to design and analyse the operation of a system, it is necessary to obtain the relevant transfer functions. For a continuous-time (CT), linear, time invariant system, also called a CT LTI system, the standard way to obtain these transfer functions is to write up the differential equations that describe the system, then take the Laplace transform of these equations, and then separate the terms such that we have the output divided by the input on the left side of the equation, and the transfer function on the right.

The stage of finding the differential equations that describe the system is called modelling the system, and it is in this step that we take the physical system and express it in the form of mathematical equations. Provided that the system to be analysed is a CT LTI system, the procedure is pretty standard and well established. If however, the system is nonlinear, or time varying, or it is analysed as a discrete-time (DT) system, then modelling it becomes a slightly more complicated operation.

As in any modelling effort, it must first be decided which of the system characteristics are important and which can be neglected. As a general engineering principle, a model should not be more complex than it needs to be. It is good protocol to start off with a simple model, examine it to make sure that it works, and then keep on adding details until the desired level of complexity is achieved. In the case of DC-to-DC converters this simple model is made up of the large signal (open loop), so-called steady state model of the converter. Once we obtain it, new components may be added to the model, or any initial approximations can be eliminated, until we end up with a small signal model that describes the closed loop, possibly nonlinear operation of the system.

The true objective is to formulate a model that takes into account all the delays and parameter fluctuations. The better the model, the higher the probability that we can design a controller that can keep the system stable, running within its optimal operating limits. Irrespective of the technique that is used to derive the model, the goal is to achieve the small signal model, ideally with as few simplifying approximations as possible.

Obtaining a good model of a switchable DC-to-DC converter is no trivial matter. The chief aspect that makes it a complex task is the converter's inherently nonlinear nature. Now, it is not impossible to model nonlinear systems by applying the same procedures that one uses for linear systems, but the necessary approximations that such a technique comes with, result in neglecting a substantial part of the dynamic behaviour of the nonlinear system. In other words, all systems can be modelled by following the procedure put in place by Middelbrook and Wester in the early seventies[8] - the state space averaging technique. This method is well structured, circuit based, control design friendly, and easy to implement, able to be automated. Its downsides are that it relies on approximations, does not capture the dynamic nature of the converter, and it is mostly intended for the analysis of continuous-time systems.

Packard was the first to construct a discrete time model in the mid seventies, [9]. His model lacks the user-friendliness of state space averaging, put does take into account the dynamics of the switching power converter (SPC). This technique later evolved into exact sampled-data models and hybrids, which aim to find a compromise between the simplicity of the state space averaging and the accuracy of the exact discrete-time model.

According to [10], it was the above mentioned works of Middelbrook and Wester, Cuk, and Packard, that represent the origin of two trends in SPC dynamic models. One of the trends aimed at developing modelling techniques which would readily lend themselves to be used in control design, while the other focused on the goal of obtaining mathematical models that were exact, with a minimum number of approximations, but less appropriate to be used in controller design.

Before shying away from the state space averaging technique, it must be noted that it can be used and is indeed often employed to model SPCs, especially when combined with traditional industry control solutions, like PI control [11]. The parameter selection of a PI controller is a compromise between robustness, and the ability to handle transient response. Its' use can yield satisfactory results, if the converter is unlikely to be experiencing strong variations from its' intended steady state operating point. It is however specified in [12] that the use of conventional control techniques on linearized models may lead to deteriorated performance or unpredictable behaviour. The paper further stresses that, when applied on SPCs, the popular industrial control schemes, like PI, voltage mode control (VMC) and current mode control (CMC) does not guarantee performance and stability in non nominal (equilibrium/ steady state) conditions.

The discrete-time model that is derived in this paper is based on Packard's PHD dissertation from '76. The essence of the technique is to follow the evolution of the state variables during the sub-intervals of the switching cycle. Packard's original model has been thoroughly studied and refined over the years. The basis for the discrete-time model that is presented in this thesis can be found in [13]. The main idea is to derive an iterative function that expresses the state variables at a given sampling instant by using the values obtained at the preceding sampling time.

What Packard's discrete time modelling and Middelbrook, Wester, and Cuk's state space

averaging technique have in common is that they make use of the canonical form, as it is tidy, well structured, easy to follow, and can be applied to all switching converters. The main characteristics of the method are:

- the order of the system is identical with the number of energy storing elements
- the energy storing elements are conventionally chosen as state space variables, as it is these elements that function as the memory of the system, making possible to do the energy accounting as the system moves through its states
- the increase in the number of inputs and/ or outputs does not complicate the calculations, due to the ingenuity of the canonical form
- when increasing the order of the system by adding another energy storing component, we just increment the state variables vector by 1, and in practice this translates to adding one extra first order differential equation

As the method originated from the state space averaging technique, there are several requirements that must be observed. As explained in [14], to satisfy the continuity requirement, the natural, modulation signal frequencies must be sufficiently low with respect to the switching frequency. As for the linearity requirement, it can be satisfied by making sure that the time variations of the relevant variables, from the steady state operation point, are kept small. In essence, the size of our focus must be large in comparison to the size of the discrete parts - much like we perceive the continuity of the light being emitted by an incandescent light bulb, or the texture of a computer screen appears to be one contiguous surface when the pixel quantity and playback frequency are high enough.

Structurally, the mathematical expressions that make up the model are grouped together in functional units, in the form of four matrices and four vectors:

- one matrix containing the parameters pertaining to the energy storing components of the system, commonly referred to as the system matrix, $\mathbf{A}$
- one containing parameters pertaining to the input variables, usually called matrix $\mathbf{B}$
- one matrix that contains measured values of the state variables, possibly referred to as $\mathbf{C}$
- one matrix that contains measured values of the input variables, possibly referred to as $\mathbf{D}$
- one column vector contains the state variables, commonly referred to as x
- one column vector contains the derivatives of the state variables, commonly referred to as $\dot{x}$

- one column vector contains the input variables, normally referred to as u
- one column vector contains the measured variables at the output, normally referred to as y

With the help of the above mentioned structural components, it is possible to express any switching converter in the short and tidy form of two equations:

$$\begin{aligned} \dot{x} &= \mathbf{A}x + \mathbf{B}u \\ y &= \mathbf{C}x + \mathbf{D}u \end{aligned} \tag{12}$$

3.2 Considerations on the nonlinearity of SPCs

One of the earliest papers that touched on the subject of nonlinearity in SPCs, [15], pointed out that most of the dynamical systems that surround us are nonlinear. The solar system, the weather, population dynamics, the economy, power electronics circuits, all are systems governed by nonlinear differential or difference equations. According to [10], any system that has a set of independent state variables that have a deterministic interaction between them and the system's inputs, can be called a dynamical system.

The weakly nonlinear nature of a system can be dealt with by linearizing around a nominal operating point, with the goal of obtaining a small signal model - exactly like in the state space averaging is applied to the analysis of switched power electronic converters.

Deane and Hamill state that there are multiple possible sources of nonlinear behaviour in power electronic systems: semiconductor devices (switches modelled as ideal switches), nonlinear capacitances, for example MOSFET capacitances, nonlinear inductances (like those of transformers), control circuits (comparators, PWM, multipliers, phase locked loops, digital controllers).

The main consequence of ignoring nonlinear behaviour is the loss of stability, such that the system starts operating chaotically. Dean and Hamill define chaos as "a noise-like, bounded oscillation with an infinite period, found in nonlinear, deterministic systems. It is characterised by extreme sensitivity to initial conditions, in such that infinitesimal perturbation of initial conditions gives rise to macroscopically diverging solutions".

In [10] they use slightly more scientific wording to define the main elements of nonlinearity and chaos. The nonlinear system is said to require analysis of higher complexity, when compared to linear systems. The steady state that the system enters after having passed through the transient period, is called an attractor. Convergence to a steady state, in the case of a nonlinear system, will depend on the initial conditions of the state variables. There are several types of attractors:

- if the steady state solution of the system is one point in the state space, the attractor is called an *equilibrium point*

- if the steady state solution moves along a closed trajectory in state space, the attractor is called a *limit cycle, or a periodic orbit*
- if the steady state trajectory of the system moves along the surface of a torus, the attractor is called a *quasi-periodic attractor*
- if the steady state of the system follows no closed trajectory, and it jumps around in the state space without any periodicity, then the attractor is *a chaotic attractor*

Switched mode dc-dc converters are nonlinear systems under feedback control, and as such, they present many opportunities for chaotic operation. Pulse width modulation is inherently nonlinear, as whatever the input, the duty factor of the output must be between 0 and 1.

If the parameters of a nonlinear system are varied, it may lead to a sudden change of qualitative behaviour of the system. This is commonly referred to as a bifurcation. There are several tools that allow for the visualisation of nonlinear behaviour, and the best suited tool to observe bifurcations is a bifurcation diagram.

The most often used equation to exemplify a bifurcation diagram, is the logistic equation:

$$x_{n+1} = rx(1 - x) \tag{13}$$

where x_{n+1} is the future value of the size of a given population, x is the present value, synonymous to the initial condition value in the case of an ODE, and r is the growth rate of the population in discussion. By running the calculation of the equation recursively many times, the result will gravitate to one certain attractor, the steady state of the system. By varying the growth rate variable, r, between 0 and 4, and running the computation until the respective steady states have been achieved, and then plotting the values of r against the values of the population size, the following diagram is obtained:

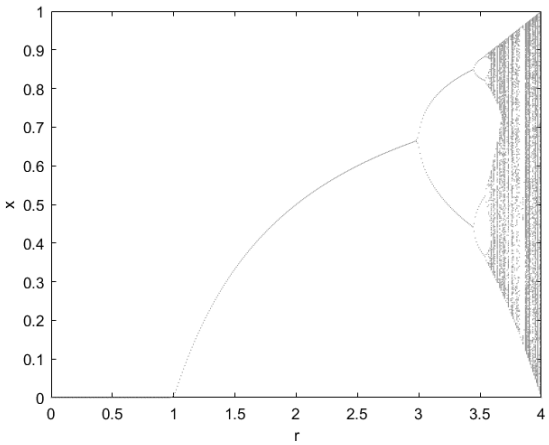

Figure 9: The bifurcation diagram of the logistic equation

Upon reading the diagram, one finds that for values of r between 0 and 1, the system will settle on a steady state point, an equilibrium point, with a value equal to 0. For values of r between 1 and 3 the size of the population is always equal to a steady state point in the state space, and it has but 1 period. At $r = 3$, the diagram shows what is called a period doubling, meaning that now the size of the population will oscillate with a periodicity of 2, between 2 steady states. This basically says that both steady state values are possible, and the value of the population size will converge on one of them. As the value of r is increased further, there is another period doubling, and then yet another one, barely visible in the diagram. At approximately $r = 3.6$ the system slips into chaos, as there are infinitely many attractors, and it is impossible to predict where the system will settle.

The period doubling bifurcation is not the only type of bifurcation that a system may experience. According to [10], these are the other two types:

- the Hopf bifurcation is characterised by a sudden birth of a limit cycle from an equilibrium point
- the saddle node bifurcation (tangent, or cyclic fold bifurcation in the case of discrete time systems), is characterised by a sudden appearance or disappearance of a pair of equilibrium points.

Furthermore, another classification of bifurcations can be made on the bases of whether or not structural changes have taken place. Bifurcations that are not brought on by any structural changes in the system are referred to as *smooth bifurcations*. On the other hand, if the bifurcations are the result of any structural changes, these are called *border collision bifurcations*.

Having listed the different types of bifurcations, it is important to note that, depending on the precursor state of the system, there are different routes to chaos:

- as it can be observed in the example presented above, as the parameter of the growth rate is modified, the system undergoes a period doubling bifurcation, which is repeated when the value of the parameter is increased, and the system does eventually end up in chaotic behaviour through *period doubling*
- alternatively, varying one parameter might result in the system experiencing Hopf bifurcation, and by continued variation of that parameter, the periodicity of the limit cycle is also modified, resulting in the system reaching a state of chaos by *quasi-periodicity*

After having presented some important aspects and characteristics of the affect of nonlinear behaviour on switched power electronic converters, the subject of control is discussed next. On a general level, there are two main goals that must be achieved through the control method [12]. A feasible control region must be specified, inside which the control

gains are capable of securing that closed-loop stability, saturation avoidance, and special bifurcation avoidance conditions are met. Then, a second control law must be put in place, whose sole objective is to maximise performance measuring metrics.

One way to attempt reaching these two goals is to simply take conventional continuous time control techniques, and convert them to discrete time, by for example converting from the Laplace domain, to the Z domain. This will, however, yield poor results, as it would entail adding even more nonlinear dynamics, due to the analogue-to-digital conversion [10].

There must therefore be other control methods, especially suited to nonlinear systems, such as model predictive control, constrained stabilisation, linear matrix inequalities convex optimisation control synthesis methods, passivity-based control [12]. This listing is far from exhaustive, and it will only be getting longer, including notable contributions from the field of AI.

The most common approach towards setting up a suitable control procedure, is to first identify the route to chaos that the system takes - plotting the bifurcation diagram, and observing at which point the system loses stability, and what is the type of bifurcation that occurs. However, in [16], D Pikulins points out that not all bifurcation detection techniques are equal in their role of control design tools. He advocates that merely observing the impact of modifying the value of one parameter does not yield satisfactory results. One must employ complete bifurcation diagrams (CBD), obtained by means of numerical calculations, continuation techniques and Floquet theory.

Generally, in [10], they argue that control methods of chaos may be classified into two different types: control achieved via external force, or via feedback control techniques. Referring to the first type, the text writes that

> "The option of adding an external signal to ensure stability has been widely used in the power converter area, especially in CMC, where FSI is exhibited in principle when the duty cycle of the control signal is above 0.5. A common way for avoiding subharmonic oscillations and chaotic regimes is by means of adding a compensating ramp to the feedback control signal Murdock (1987) and Tse and Lai (2000)."

The term FSI stands for fast-scale instabilities, and it refers to the exhibition of chaotic instabilities and subharmonic oscillations.

The Hopf bifurcation is on the other hand referred to as slow-scale instability, or SSI. This second type of instability can be controlled by the action of feedback loops, due to the option of using readily available control design oriented models, allowing frequency domain representation and relatively simple analysis techniques, like the Nyquist diagram.

When it comes to choosing between analogue and digital controllers, it appears that the ladder offers several advantages over the former [17]: improved system reliability, flexi-

bility, ease of integration and optimisation. In addition, fine tuning of the components, as well as value selection according to design specification are replaced by software programming. The authors of the paper have shown that in the case of a Buck converter, a digital controller manages to provide constant output voltage, despite of changes in various system parameters, as well as the controller's ability to provide stabilised output without external passive components. It has also been proved that the controller can stabilise chaos and noise vibrations occurring at high values of the input voltage, or other variations of the system parameters. The system is thus constrained to operate with a period 1 operation.

These paragraphs presenting some of the more important generalities of nonlinear control methods is concluded by some few observations from one of the earliest papers written on the subject. In [15], Deane and Hamill write that in 1990 the research of chaos was still in its infancy, and the passage of time has proved them right. One of their suggestions was that chaos must not necessarily be avoided at all cost, as positive results of its occurrence might also be discovered. On a side note, systems may also be deliberately constructed to operate in their chaos regions. Yet another interesting observation was that simple systems may exhibit complex behaviour, just as complex systems may exhibit simple behaviour. It is in the spirit of this final sentence, that the control method presented in this paper had been chosen.

The control method described in this paper is quite simple, and it is based on the pole placement technique. In the same time it bears strong resemblance to the method presented in article [18], included in the 2014 book entitled Applied Non-Linear Dynamics Systems. The authors of the article present a method that is based on the use of simple bifurcation diagrams, and it lends itself to be used in PWM controlled power converters.The method is called "adaptive ramp control", and it consists of adapting the ramp waveform $V_r(t)$ to the control input $V_c(t)$ in such a way that the control signal never loses contact with the ramp waveform. Practically, the goal is to maintain a functioning PWM even when the input voltage V_1 is varied, while keeping the switching frequency unchanged.

Simply put, the PWM works by comparing a control voltage with a periodic ramp waveform (voltage):

$$V_r(t) = V_L + (V_U - V_L)\frac{t}{T_s} \tag{14}$$

where V_L and V_U stands for lower, and upper voltage value, respectively, and T_s is the switching period. For visual support, refer to figure 10 below: The PWM diagram shows that whenever the control voltage is higher in amplitude than the amplitude of the ramp voltage, the switch of the converter is ON for that respective time period, also possible to be specified in degrees, hence the δ symbol in the diagram. Mathematically, this can be expressed by specifying the control output u as:

$$u = \begin{cases} 1 \; if \; V_c(t) > V_r(t) \\ 0 \; if \; V_c(t) < V_r(t) \end{cases} \tag{15}$$

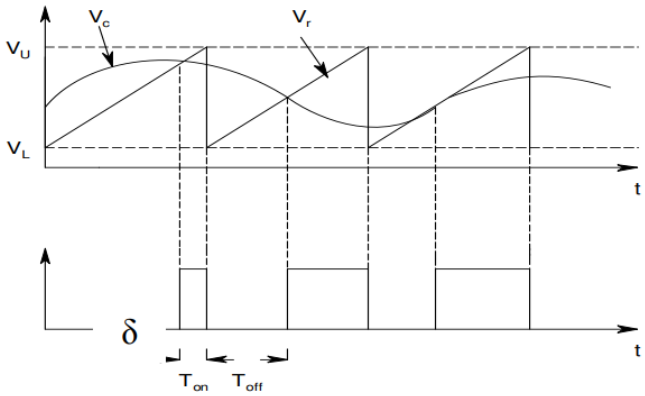

Figure 10: PWM diagram, from [15]

The control voltage V_c is proportional to the error signal, which is in turn calculated by subtracting the reference voltage V_{ref} from the output voltage V_o:

$$V_c(t) = a(V_o - V_{ref}) \tag{16}$$

where a is an amplifying gain.

The problem is that by increasing the input voltage, the control voltage is also increased, and it can no longer interact with the ramp voltage, causing the occurrence of bifurcations. The solution is then to change the value of the ramp voltage, but avoid modifying the slope of the ramp. The first step is to agree on the value of the constant slope, by observing the bifurcation diagram when the slope changes. The authors introduce the expression for the adaptive ramp, V_{ar}:

$$V_{ar} = \frac{V_c(t)}{k} + \frac{V_{in}}{k}\frac{t}{T_s} \tag{17}$$

where k is a constant that needs to be computed, and V_in is a fixed constant value. The values of these two unknown variables must be computed in such a way that 1 period operation is maintained, and the regulation performance is kept at an acceptable level. One should note that changes in the control voltage cause the adaptive ramp voltage to change its offset. The control output is now given by comparing the control voltage to the adaptive ramp signal:

$$u = \begin{cases} 1 \; if \; V_c(t) > V_{ar}(t) \\ 0 \; if \; V_c(t) < V_{ar}(t) \end{cases} \tag{18}$$

The first step is obtaining a bifurcation diagram by plotting relevant values of V_{in}, its intended working range, against relevant values of k. The highest value of the input voltage range should be chosen as V_{in} in equation 17 This diagram will show for which values of k the system will run under the 1 period requirement. The next point of interest is finding the values for which the system exhibits the lowest steady state errors. This step yields an optimal value for k, such that the only remaining unknown in equation 17

is the value of the adaptive ramp itself.

3.3 Derivation of the DAB converter model

Keeping true to the spirit of engineering, it is wise to always aim to reduce the complexity of a system. If the complexity can be reduced without compromising the model's completeness, then the resulting system will become much easier to analyse. This is the essence of finding Thevenin equivalent of an elaborate circuit.

In the case of the DAB converter, it is wise to make a series of manipulations, which allows us to reduce its complexity to the level of an ordinary buck converter. The starting point is the diagram of the DAB converter depicted in figure 1. As the current will always be flowing through 2 switches pertaining to separate legs of each bridge, it is possible to redraw the circuit diagram for each of the states:

1. We have the first state, between t_0 and t_1, when S_1, S_4, S_6 and S_7 are conducting. The circuit diagram representing this state is depicted below:

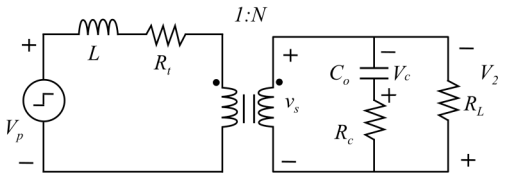

Figure 11: DAB converter diagram representing the first

2. We consider the second state between t_1 and t_2, when it is switches S_1, S_4, S_5 and S_8 that are conducting the current. The circuit diagram that describes this state is drawn below:

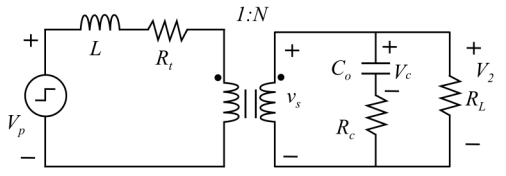

Figure 12: DAB converter diagram representing the second state

3. The third state spans the time period between t_2 and t_3 and the current is passing through switches S_2, S_3, S_5 and S_8.

   The circuit diagram of the third state is identical to that pertaining to the second state, but the input voltage $V_1 = V_p$ now has a negative sign.

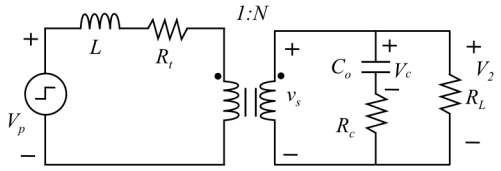

Figure 13: DAB converter diagram representing the third state

4. The fourth state of under SPS modulation is between t_3 and t_4, when the current passes through S_2, S_3, S_6 and S_7:

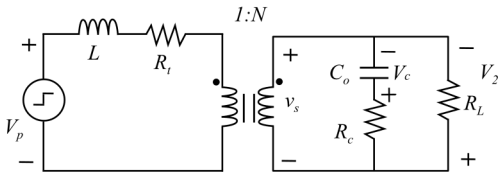

Figure 14: DAB converter diagram representing the fourth state

The circuit diagram of the DAB converter in this state is identical to the one representing the first state, but also here, as in the preceding state, V_p has a negative sign.

If we now refer the leakage inductance and the resistance representing the copper loss from the primary to the secondary, as well as the primary voltage source, such that all our parameters are contained in the secondary bridge, we end up with the following circuit diagram:

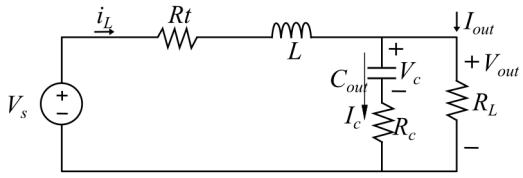

Figure 15: The Buck equivalent model of the DAB converter in states 2 and 3

This image is identical with the circuit diagram of a Buck converter during its ON state, with the copper loss and capacitor ESR included. The DAB converter has no OFF states, as there will always be 2 pairs of switches conducting the current, so the OFF state of the Buck converter is of no special interest at this stage.

Next, the detailed derivation of a discrete-time (DT) model for the simple Buck converter is employed, as this will serve as a basis for the DT model of the DAB converter. The derivation processes are similar, but where the Buck converter only has 2 states (switch ON

or OFF), the DAB converter will either have 4 states, in the case of the SPS modulation, or 6 states for the EPS modulation technique. It is therefore advantageous to show the procedure in detail for the simple case, and then tweak and adapt the model to the more complex structure of the DAB converter.

3.3.1 The simple model of a Buck converter

Starting with a generic model of a Buck converter, with copper loss and capacitor ESR included:

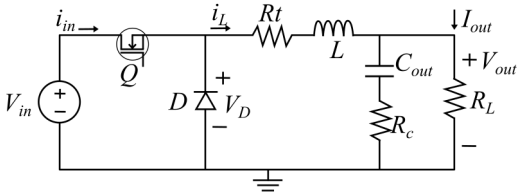

Figure 16: the Buck converter

When the switch is ON we obtain the structure depicted above, in figure 15:

As for any other switching converter, we are interested in developing the governing equations for the energy storing components, which, in this case, are the inductor current and capacitor voltage.

To conduct the circuit analysis the following specifications are made:

- the signs of the input voltage, capacitor voltage and output voltage are kept unchanged, and the currents are related to them
- the circuit diagram is divided into 2 loops in which the inductor current and output current are circulating and the loop current analysis technique is employed
- the direction of the capacitor current i_c is chosen to be out of the upper node, such that $i_L = i_c + i_o$; the end result of the derivation would be unchanged, even if the current was chosen to flow in the opposite direction, provided that we remembered to consider the sign of the capacitor current with respect to the voltage over the capacitor

For the first loop we have the following equation:

$$\begin{aligned} &-V_s + i_L R_t + V_L + V_c + R_c(i_L - i_o) = 0 \Leftrightarrow \\ &V_L = V_s - i_L R_t - V_c - R_c(i_L - i_o) \Leftrightarrow \\ &V_L = V_s - i_L(R_t + R_c) - V_c + R_c i_o \end{aligned} \tag{19}$$

Looking at the second loop now:

$$
\begin{aligned}
&V_2 + R_c(i_o - i_L) - V_c = 0 \Leftrightarrow V_2 + R_c i_o - R_c i_L - V_c = 0 \Leftrightarrow \\
&i_o R_o + R_c i_o - R_c i_L - V_c = 0 \Leftrightarrow i_o(R_o + R_c) - R_c i_L - V_c = 0 \Leftrightarrow \\
&i_o(R_o + R_c) = V_c + R_c i_L \Leftrightarrow (i_L - i_c)(R_o + R_c) = V_c + R_c i_L \Leftrightarrow \\
&i_L R_o + i_L R_c - i_c R_o - i_c R_c = V_c + R_c i_L \Leftrightarrow \\
&i_c(-R_o - R_c) = V_c + R_c i_L - i_L R_o - i_L R_c \Leftrightarrow \\
&i_c(R_o + R_c) = -V_c - R_c i_L + i_L R_o + i_L R_c \Leftrightarrow \\
&i_c(R_o + R_c) = i_L(-R_c + R_o + R_c) - V_c \Leftrightarrow \\
&i_c(R_o + R_c) = i_L R_o - V_c \implies \\
&\boxed{i_c = \mathbf{C}\frac{\mathbf{dV_c}}{\mathbf{dt}} = i_L \frac{R_o}{R_o + R_c} - V_c \frac{1}{R_o + R_c}}
\end{aligned}
\tag{20}
$$

Inserting the expression for the output current in equation 19 , $i_o = i_L - i_c$, we obtain that:

$$
\begin{aligned}
V_L &= V_s - i_L(R_t + R_c) - V_c + R_c(i_L - i_c) \Leftrightarrow \\
&= V_s - i_L R_t - V_c - R_c i_c
\end{aligned}
\tag{21}
$$

and by replacing i_c with the expression derived above, we write that

$$
\begin{aligned}
V_L &= V_s - i_L R_t - V_c - R_c(i_L \frac{R_o}{R_o + R_c} - V_c \frac{1}{R_o + R_c}) \\
&= V_s - i_L R_t - V_c - i_L \frac{R_c R_o}{R_o + R_c} + V_c \frac{R_c}{R_o + R_c} \\
&= V_s + i_L(-R_t - \frac{R_c R_o}{R_c + R_o}) + V_c(-1 + \frac{R_c}{R_c + R_o}) \Leftrightarrow \\
L\frac{di_L}{dt} &= V_s + i_L(-R_t - \frac{R_c R_o}{R_c + R_o}) + V_c(-1 + \frac{R_c}{R_c + R_o}) \Leftrightarrow \\
\frac{di_L}{d_t} &= \frac{V_s}{L} + i_L(-\frac{R_t}{L} - \frac{R_c R_o}{L(R_c + R_o)}) + V_c(\frac{-(R_o + R_c) + R_c}{L(R_o + R_c)}) \Leftrightarrow \\
&\boxed{\frac{\mathbf{di_L}}{\mathbf{d_t}} = \frac{V_s}{L} + i_L(-\frac{R_t}{L} - \frac{R_c R_o}{L(R_c + R_o)}) + V_c(-\frac{R_o}{L(R_o + R_c)})}
\end{aligned}
\tag{22}
$$

The following derivation of differential equations for **the OFF state of the converter** has a less noticeable connection to the DAB converter due to the lack of an OFF state in the DAB converter, but carrying it out is necessary nonetheless, and its usefulness will be made clear. We start the derivation by observing the circuit diagram of the Buck converter in the OFF state, and doing the loop analysis:

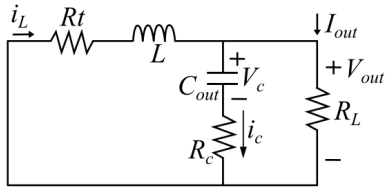

Figure 17: Buck converter circuit diagram in the OFF state

By observing the first loop, it is possible to write up the following equation:

$$\begin{aligned} &i_L R_t + V_L + V_c + R_c(i_L - i_o) = 0 \Leftrightarrow \\ &i_L R_t + V_L + V_c + R_c(i_L - (i_L - i_c) = 0 \Leftrightarrow \\ &i_L R_t + V_L + V_c + R_c i_c = 0 \Leftrightarrow \\ &V_L = -i_L R_t - V_c - R_c i_c \end{aligned} \tag{23}$$

The expression for i_c can be obtained by examining the second loop. As this second loop is identical with the second loop of the Buck converter circuit describing the ON state, it is reasonable to conclude that the expressions of the current passing through the capacitor will be identical to one-another:

$$\boxed{\mathbf{i_c} = \mathbf{C}\frac{\mathbf{dV_c}}{\mathbf{dt}} = i_L \frac{R_o}{R_o + R_c} - V_c \frac{1}{R_o + R_c}} \tag{24}$$

Replacing i_c in the expression of the voltage over the inductor we arrive to the following equation:

$$\begin{aligned} V_L &= -R_t i_L - V_c - R_c(i_L \frac{R_o}{R_o + R_c} - V_c \frac{1}{R_o + R_c}) \\ &= -R_t i_L - V_c - i_L \frac{R_o R_c}{(R_o + R_c)} + V_c \frac{R_c}{(R_o + R_c)} \Leftrightarrow \\ \frac{di_L}{dt} &= i_L(-\frac{R_t}{L} - \frac{R_o R_c}{L(R_c + R_o)}) + V_c(-\frac{-1}{L} + \frac{R_c}{L(R_c + R_o)}) \\ &= i_L(-\frac{R_t}{L} - \frac{R_o R_c}{L(R_c + R_o)}) + V_c(\frac{-R_c - R_o + R_c}{L(R_c + R_o)}) \Leftrightarrow \\ \boxed{\frac{\mathbf{di_L}}{\mathbf{dt}} &= i_L(-\frac{R_t}{L} - \frac{R_o R_c}{L(R_c + R_o)}) + V_c(-\frac{R_o}{L(R_c + R_o)})} \end{aligned} \tag{25}$$

Having obtained the expressions for voltage over the inductor and current through the capacitor during both the ON-and OFF states of the Buck converter, we can now compose

the state matrices. The matrices pertaining to the ON state are presented first:

$$\mathbf{A_1} = \begin{bmatrix} -\frac{R_t}{L} - \frac{R_c R_o}{L(R_c + R_o)} & -\frac{R_o}{L(R_c + R_o)} \\ \frac{R_o}{C(R_c + R_o)} & -\frac{1}{C(R_c + R_o)} \end{bmatrix} \tag{26}$$

$$\mathbf{B_1} = \begin{bmatrix} \frac{1}{L} \\ 0 \end{bmatrix} \tag{27}$$

$$\mathbf{C_1} = \begin{bmatrix} \frac{R_c R_o}{R_c + R_o} & \frac{R_o}{R_c + R_o} \end{bmatrix} \tag{28}$$

$$\mathbf{D_1} = 0 \tag{29}$$

Next, the state matrices describing the dynamics of the OFF state are composed as follows:

$$\mathbf{A_2} = \begin{bmatrix} -\frac{R_t}{L} - \frac{R_c R_o}{L(R_c + R_o)} & -\frac{R_o}{L(R_c + R_o)} \\ \frac{R_o}{C(R_c + R_o)} & -\frac{1}{C(R_c + R_o)} \end{bmatrix} \tag{30}$$

$$\mathbf{B_0} = \begin{bmatrix} \mathbf{0} \end{bmatrix} \tag{31}$$

$$\mathbf{C_2} = \begin{bmatrix} \frac{R_c R_o}{R_c + R_o} & \frac{R_o}{R_c + R_o} \end{bmatrix} \tag{32}$$

$$\mathbf{D_1} = \mathbf{0} \tag{33}$$

The observant reader will notice that the **A**, **C**, and **D** matrices are identical, while the **B** matrices are different from each other.

One practical way of verifying the correctness of the model, is to set the value of the capacitor ESR to 0, and check if the resulting expressions match the ones derived for a buck converter where the copper loss and the capacitor ESR are ignored.

Given that the goal is to determine a discrete-time model of the DAB converter, it is now the point for the discrete notation to be introduced. Instead of writing:

$$\begin{aligned} \dot{x} &= \mathbf{A}x + \mathbf{B}u \\ y &= \mathbf{C}x + \mathbf{D}u \end{aligned} \tag{34}$$

we can now write:

$$\begin{aligned} \mathbf{x}(k+1) &= \mathbf{G}\mathbf{x}(k) + \mathbf{H}\mathbf{u}(k) \\ \mathbf{y}(k) &= \mathbf{C}\mathbf{x}(k) + \mathbf{D}\mathbf{u}(k) \end{aligned} \tag{35}$$

As the system under study is a time-variant system, matrices $\mathbf{A}$ and $\mathbf{G}$ are identical, made up of constant coefficients. If we regard the input as being the control signal, then also matrices $\mathbf{B}$ and $\mathbf{H}$ will be identical.

The solution in this case for any positive integer k may then be obtained by recursion[19]:

$$\begin{aligned} &\mathbf{x}(1) = \mathbf{A}\mathbf{x}(0) + \mathbf{B}\mathbf{u}(0) \\ &\mathbf{x}(2) = \mathbf{A}\mathbf{x}(1) + \mathbf{B}\mathbf{u}(1) = \mathbf{A^2}\mathbf{x}(0) + \mathbf{A}\mathbf{B}\mathbf{u}(0) + \mathbf{B}\mathbf{u}(1) \\ &\mathbf{x}(3) = \mathbf{A}\mathbf{x}(2) + \mathbf{B}\mathbf{u}(2) = \mathbf{A^3}\mathbf{x}(0) + \mathbf{A^2}\mathbf{B}\mathbf{u}(0) + \mathbf{A}\mathbf{B}\mathbf{u}(1) + \mathbf{B}\mathbf{u}(2) \\ &..... \\ &\mathbf{x}(k) = \mathbf{A^k}\mathbf{x}(0) + \sum_{j=0}^{k-1} \mathbf{A}^{k-j-1}\mathbf{B}\mathbf{u}(j) \quad k = 1, 2, 3... \end{aligned} \tag{36}$$

and for the output, it can be written as:

$$\mathbf{y}(k) = \mathbf{C}\mathbf{A}^k\mathbf{x}(0) + C\sum_{j=0}^{k-1} \mathbf{A}^{k-j-1}\mathbf{B}\mathbf{u}(j) + \mathbf{D}\mathbf{u}(k) \tag{37}$$

By introducing now the *state transition matrix*

$$\mathbf{\Psi}(k) = \mathbf{A}^k \tag{38}$$

it is possible to rewrite the generic solution of the linear time-invariant discrete-time state equation as:

$$\begin{aligned} \mathbf{x}(k) &= \mathbf{\Psi}(k)\mathbf{x}(0) + \sum_{j=0}^{k-1} \mathbf{\Psi}^{k-j-1}\mathbf{B}\mathbf{u}(j) \\ &= \mathbf{\Psi}(k)\mathbf{x}(0) + \sum_{j=0}^{k-1} \mathbf{\Psi}(j)\mathbf{B}\mathbf{u}(k-j-1) \end{aligned} \tag{39}$$

with the output given as:

$$\begin{aligned}\mathbf{y}(k) &= \mathbf{C}\boldsymbol{\Psi}(k)\mathbf{x}(0) + C\sum_{j=0}^{k-1}\boldsymbol{\Psi}(k-j-1)\mathbf{B}\mathbf{u}(j) + \mathbf{D}\mathbf{u}(k) \\ &= \mathbf{C}\boldsymbol{\Psi}(k)\mathbf{x}(0) + C\sum_{j=0}^{k-1}\boldsymbol{\Psi}(j)\mathbf{B}\mathbf{u}(k-j-1) + \mathbf{D}\mathbf{u}(k)\end{aligned} \tag{40}$$

The essence of discrete-time modelling is that we want to be able to know the state of the system at each shift in internal states during any given switching cycle. To achieve this goal, the state variables vector will be calculated as often as needed, at least once per internal state, and at the end of each cycle. Just like in the case of CT systems, the values of the state variables are made up of the interaction between the energy storing components, and the effect of the input variables.

We thus have that for the two states of the Buck converter we have the following expressions:

$$\begin{aligned}\mathbf{x}_{n1} = f_{n1}(\mathbf{x}_n, d_n) = e^{\mathbf{A_1}t_{n1}}\mathbf{x}_n + \boldsymbol{\Psi}_\mathbf{1}V_{in} \Leftrightarrow \\ \mathbf{x}(nT_s + t_{on}) = e^{\mathbf{A_1}t_{on}}\mathbf{x}(nT_s) + \boldsymbol{\Psi}_\mathbf{1}V_{in}\end{aligned} \tag{41}$$

and

$$\begin{aligned}\mathbf{x}_{n+1} = f_{n2}(\mathbf{x}_{n2}, d_n) = e^{\mathbf{A_2}t_{n2}}\mathbf{x}_{n2} + \boldsymbol{\Psi}_\mathbf{1}V_{in} \Leftrightarrow \\ \mathbf{x}((n+1)T_s) = e^{\mathbf{A_2}t_{n2}}\mathbf{x}(nT_s + t_{on}) + \boldsymbol{\Psi}_\mathbf{2}V_{in}\end{aligned} \tag{42}$$

Based on the conventional techniques for solving time variant systems of differential equations, as presented in [19] and [8], it is an advantage if the solving procedure is structured, tidy, and easy to follow. It is therefore desired to keep the well known form of expression 12:

$$\mathbf{x}(n+1) = \mathbf{F}(d_n)\mathbf{x}_n + \mathbf{G}(d_n)V_{in} \tag{43}$$

The first term in the equation can be referred to as the state propagation matrix,[20], and it encompasses the dynamic interaction of the state variables in the underlying (preceding) cycle, while the second term represents the effect of the input variables. "d_n" represents the dynamic duty ratio, and is basically the only control variable, through which it is possible to obtain the desired output parameters.

Taking a closer look at the F matrix, one should note that it is expressed as follows:

$$\begin{aligned}\mathbf{F}(d_n) = e^{\mathbf{A_2}t_{n2}} \cdot e^{\mathbf{A_1}t_{n1}} \Leftrightarrow \\ \mathbf{F}(d_n) = e^{\mathbf{A_2}t_{n2}} \cdot e^{\mathbf{A_1}t_{on}}\end{aligned} \tag{44}$$

The $\mathbf{G}$ vector is slightly more complex in its composition:

$$\mathbf{G}(d_n) = e^{\mathbf{A_2}t_{n2}} \cdot \mathbf{\Psi_1} + \mathbf{\Psi_2} \tag{45}$$

where Ψ_1 and Ψ_2 are calculated as follows:

$$\begin{aligned} \mathbf{\Psi_1} &= \int_0^{t_1} e^{\mathbf{A_1}\tau}\mathbf{B_1}d\tau = \mathbf{A_1}^{-1}[e^{\mathbf{A_1}\tau}]_0^{t_{on}}\mathbf{B_1} \\ &= \mathbf{A_1}^{-1}(e^{\mathbf{A_1}t_{on}} - I)\mathbf{B_1} \end{aligned} \tag{46}$$

$$\begin{aligned} \mathbf{\Psi_2} &= \int_0^{t_2} e^{\mathbf{A_2}\tau}\mathbf{B_2}d\tau = \mathbf{A_2}^{-1}[e^{\mathbf{A_2}\tau}]_0^{t_{n2}}\mathbf{B_2} \\ &= \mathbf{A_2}^{-1}(e^{\mathbf{A_2}t_{n2}} - I)\mathbf{B_2} \end{aligned} \tag{47}$$

Note that most of the variables involved in the expressions above are of a constant nature. It is indeed only the variables specifying the time periods for the ON-time and OFF-time of the switches that can vary from cycle-to-cycle, as they depend on the appropriate duty ratio. The duty ratio is in turn specified based on the error obtained by subtracting the value of the feedback voltage from the reference voltage. The time periods are therefore expressed as:

$$\begin{aligned} t_{n1} &= t_{on} = d_n \cdot T_s \\ t_{n2} &= t_{off} = (1 - d_n) \cdot T_s \end{aligned} \tag{48}$$

To check the correctness of the DT model, a simple proportional controller is employed. Its effect is desired to be similar to a simplified pole placement, which in turn is a version of the root locus design technique. Pole placement techniques are employed to design appropriate control procedures with the ability to control the system in both static and dynamic state feedback situations[12].

The main idea is to obtain the desired response of a system by manipulating the placement of the poles of the transfer function, which are identical to the eigenvalues of the transition matrix. The feedback loop depicted below in figure 18 will aid in acquiring a swift understanding of the control technique:

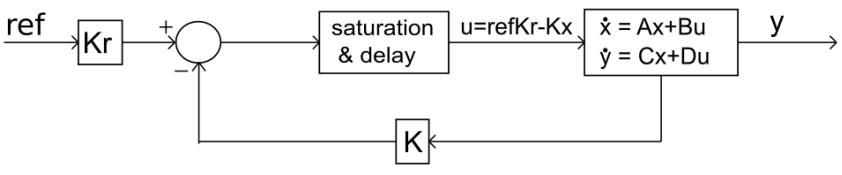

Figure 18: 2 gains feedback loop for pole placement

Instead of feeding back the output y as in conventional PID control, it is the state space column vector that is fed back, after being adjusted by the gain K. The role of this

gain is to stabilise the system, making sure that the eigen values (poles) will be situated inside the left half side of the complex plane (or inside the unite circle if a z-transform is employed), at the desired distance from the origin, as dictated by the desired response speed. The reference is also passed through a gain, K_r, the role of which is to eliminate any steady state error. The new control variable is then sent to into the plant in order to obtain the new state space values. Note the presence of the saturation and delay block - making sure that the control impulse stays within the actuator's limits, and serving as a reminder that the control system is operating with the delay of 1 switching cycle.

Another version of this control method, the one that is employed in the writing of this thesis, is based on the block diagram depicted below, in figure 19:

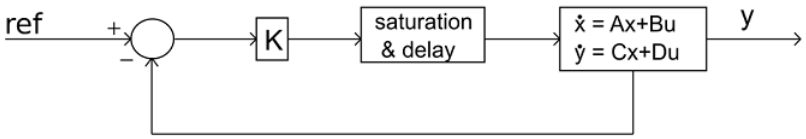

Figure 19: Single gain version of the pole placement method

Under this setup the values of the state space variables are again fed back, but now they are first subtracted from the reference value, and then the proportional gain is applied. The resulting control signal is then fed to the plant to calculate the state space variable values of the subsequent cycle. Again, the controller operates with the delay of 1 switching cycle, and saturation limiter is implemented as well. The role of K in this second configuration is to secure system stability, as well as keeping the steady state error of the system within acceptable boundaries. The mechanics of the controller are encompassed in the following mathematical expression:

$$d_{n+1} = k(V_{ref,n} - V_{2,n}) \tag{49}$$

As we are only interested in regulating the output voltage V_2, it can be defined as:

$$\begin{aligned}
V_2 &= V_c + V_{R_c} = V_c + i_c R_c \\
i_c &= i_L \frac{R_o}{R_c + R_o} - V_c \frac{1}{R_c + R_o} \implies \\
V_2 &= V_c + R_c(i_L \frac{R_o}{R_c + R_o} - V_c \frac{1}{R_c + R_o}) \\
&= V_c + i_L \frac{R_c R_o}{R_c + R_o} - V_c \frac{R_c}{R_c + R_o} \\
&= i_L \frac{R_c R_o}{R_c + R_o} + V_c(1 - \frac{R_c}{R_c + R_o}) \\
&= i_L \frac{R_c R_o}{R_c + R_o} + V_c \frac{R_o}{R_c + R_o}
\end{aligned} \tag{50}$$

and this is the same as $\mathbf{C_1}$ and $\mathbf{C_2}$ multiplied with the state space column vector.

This allows us to express equation 49 as:

$$d_{n+1} = k(V_{ref,n} - (\frac{R_c R_o}{R_c + R_o} + \frac{R_o}{R_c + R_o})\mathbf{x}_n) \tag{51}$$

As mentioned before, there are two goals that that the controller must deliver: the system must be stable, and the steady state error must be kept under a maximum accepted value. This paper focuses on assessing the stability of the system. Given that the controller is a simple proportional controller, some steady state error must be tolerated. The value of the proportional gain K is first an foremost chosen to satisfy the stability conditions of the model.

Built on the state space modelling studies of switched converters stretching back to the seventies, like [9] and [8], in [21] the stability of the system is verified as described below. Firstly, the main are equations listed below:

$$\boxed{\begin{aligned} i_{L(n+1)} &= [10]\mathbf{x}_{n+1} \\ v_{c(n+1)} &= [01]\mathbf{x}_{n+1} \\ d_{(n+1)} &= k(V_{ref,n} - V_{2,n}) \\ d_{(n+1)} &\in [0,1] \end{aligned}} \tag{52}$$

Next, the Jacobian matrix is constructed:

$$J(I_L, V_c, D) = \begin{bmatrix} \frac{\partial i_{L(n+1)}}{\partial i_{Ln}} & \frac{\partial i_{L(n+1)}}{\partial v_{cn}} & \frac{\partial i_{L(n+1)}}{\partial d_n} \\ \frac{\partial v_{c(n+1)}}{\partial i_{Ln}} & \frac{\partial v_{c(n+1)}}{\partial v_{cn}} & \frac{\partial v_{c(n+1)}}{\partial d_n} \\ \frac{\partial d_{(n+1)}}{\partial i_{Ln}} & \frac{\partial d_{(n+1)}}{\partial v_{cn}} & \frac{\partial d_{(n+1)}}{\partial d_n} \end{bmatrix} \tag{53}$$

where the capital letters I_L, V_c, D denote the steady state values of the inductor current, capacitor voltage and duty ratio, respectively.

The determinant of the Jacobian is then computed and locally asymptotic stability is recognised provided that none of the resulting eigen values have an absolute value greater than 1 [15], [10], [8]:

$$det(\lambda I - J(I_L, V_c, D)) = 0 \tag{54}$$

If the eigenvalues have a magnitude larger than 1 (also signifying that it crosses the

unit circle in discrete time systems, or it is situated in the right half plain in the case of continuous time systems), it is possible to determine what kind of instability the system is experiencing by observing the nature of the eigenvalues [10]. If they have imaginary terms, then a Hopf bifurcation, or in the case of discrete time systems, a so called Neimark-Sacker bifurcation, will occur. If, however, one eigenvalues crosses the unit circle at -1, one will notice that the system undergoes period doubling bifurcation. If the eigenvalue crosses the unit circle at a value equal to 1, a saddle node bifurcation will be observed.

3.3.2 The discrete time model under SPS modulation

The diagram of the DAB converter depicted in figure 20 **without** taking into account $\mathbf{R_t}$, which is the total copper resistance, **and** $\mathbf{R_c}$, which is the resistance of the output capacitor.

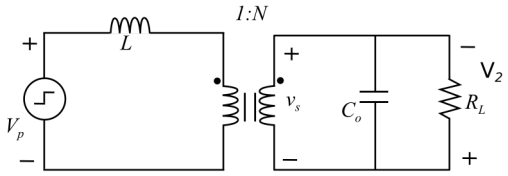

Figure 20: The simplified diagram of a DAB converter, ignoring R_t andR_c

This is the expression for the inductor voltage:

$$V_L = V_p - \frac{v_s}{N} \Leftrightarrow L\frac{di_L}{dt} = V_p - \frac{v_s}{N} \Leftrightarrow \frac{di_L}{dt} = \frac{1}{L}V_p + \frac{1}{NL}v_s = \frac{1}{L}V_p + \frac{1}{NL}V_c$$

As for the capacitor current, using the transformer's property according to which:

$$\frac{i_{L1}}{i_{L2}} = \frac{N_2}{N_1} = \frac{N}{1} \implies i_{L2} = \frac{i_{L1} \cdot 1}{N} = i_{L1} \cdot \frac{1}{N} \tag{55}$$

where i_{L1} is current running through the inductor on the primary side, and i_{L2} is the inductor current referred to the secondary side.

Now, having that:

$$i_c = C\frac{dV_c}{dt} \tag{56}$$

Using KCL, following mathematical formulation can be set up:

$$\begin{aligned} &i_{L2} = i_{L1} \cdot \frac{1}{N} = i_C + i_o = C\frac{dV_c}{dt} + \frac{V_c}{R_o} \implies \\ &C\frac{dV_c}{dt} = i_{L1} \cdot \frac{1}{N} - \frac{V_c}{R_o} \implies \frac{dV_c}{dt} = i_{L1} \cdot \frac{1}{NC} - \frac{V_c}{R_oC} \end{aligned} \tag{57}$$

From the above equations it then follows that:

$$\begin{bmatrix} i_L \\ V_c \end{bmatrix} = \begin{bmatrix} 0 & \frac{1}{NL} \\ -\frac{1}{NC} & -\frac{1}{R_L C} \end{bmatrix} \begin{bmatrix} i_L \\ V_c \end{bmatrix} + \begin{bmatrix} \frac{1}{L} \\ 0 \end{bmatrix} V_p \tag{58}$$

Now, the resistance of the wires, the copper resistance, $\mathbf{R_t}$, **and** the resistance of the capacitor, $\mathbf{R_c}$ **are included** in the diagram, and the new equations are derived. The new circuit representation is depicted below:

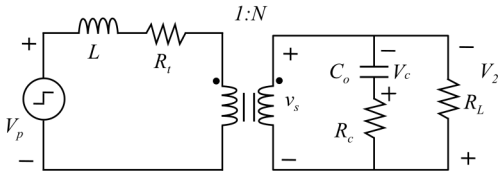

Figure 21: The DAB converter, including R_t and R_c

Starting off with the inductor voltage, we have the following:

$$V_L = L\frac{di_L}{dt} = V_p - V_R - \frac{v_s}{N} \tag{59}$$

where

$$v_s = -(V_c - i_C \cdot R_c) = -(V_c + C\frac{dV_c}{dt}R_c) \tag{60}$$

such that

$$V_L = L\frac{di_L}{dt} = V_p - i_{L1}R_t + \frac{V_c + C\frac{dV_c}{dt}R_c}{N} \tag{61}$$

and finally obtaining that:

$$\frac{di_L}{dt} = \frac{1}{L}V_p - \frac{1}{L}i_L R_t + \frac{1}{NL}V_c + \frac{C}{NL}\frac{dV_c}{dt}R_c \tag{62}$$

Pausing the further derivation of this equation, and moving on to find and expression for the capacitor current. Starting with KCL:

$$\frac{i_L}{N} = i_c - i_o \implies i_c = i_L\frac{1}{N} + i_o \tag{63}$$

Now, i_L of the primary side, referred to the secondary. becoming $i_{L2} = \frac{i_L}{N}$, such that we now have that

$$i_c = -\frac{1}{N} i_L + i_o \tag{64}$$

and i_o can be written as $\frac{V_2}{R_o}$. And since V_2 is corresponds to the voltage over the capacitor and its resistance, it can be stated that

$$V_2 = V_c - V_{ESR} \tag{65}$$

such that

$$i_c = i_L \frac{1}{N} + \frac{(V_c - i_c R_c)}{R_o} = i_L \frac{1}{N} + \frac{V_c}{R_o} - \frac{i_c R_c}{R_o} \tag{66}$$

yielding:

$$i_c + \frac{i_c R_c}{R_o} = i_L \frac{1}{N} + \frac{V_c}{R_o} \implies i_c(1 + \frac{R_c}{R_o}) = i_L \frac{1}{N} + \frac{V_c}{R_o} \tag{67}$$

which allows for i_c to be defined as:

$$i_c = \frac{i_L \frac{1}{N}}{(1 + \frac{R_c}{R_o})} + \frac{\frac{V_c}{R_o}}{(1 + \frac{R_c}{R_o})} \tag{68}$$

And since i_C can also be written as - $C\frac{dV_c}{dt}$, :

$$\boxed{\frac{dV_c}{dt} = -\frac{R_o i_L}{NC(R_o + R_c)} - \frac{V_c}{C(R_o + R_c)}} \tag{69}$$

Having obtained an appropriate expression for the capacitor current, it can now be substituted in the equation describing the inductor voltage, resulting in the following equation:

$$\frac{di_L}{dt} = \frac{1}{L} V_p - \frac{1}{L} i_L R_t + \frac{1}{L} V_c - \frac{R_o i_L}{NC(R_o + R_c)} - \frac{V_c}{C(R_o + R_c)} \tag{70}$$

This can then be written as:

$$\begin{aligned}
&\frac{di_L}{dt} = \frac{1}{L}V_p - \frac{i_L}{L}(R_t + \frac{R_cR_o}{N^2(R_o+R_c)}) + \frac{V_c}{L}(\frac{1}{N} - \frac{R_c}{N(R_o+R_c)}) \implies \\
&\frac{di_L}{dt} = \frac{V_p}{L} - i_L\frac{R_tLN^2(R_o+R_c) + R_cR_oL}{L^2N^2(R_o+R_c)} + V_c\frac{LN(R_o+R_c) - NLR_c}{N^2L^2(R_o+R_c)} \implies \\
&\boxed{\frac{di_L}{dt} = \frac{V_p}{L} - i_L\frac{R_tN^2 + \frac{R_cR_o}{(R_o+R_c)}}{L^2N^2} + V_c\frac{R_o}{NL(R_o+R_c)}}
\end{aligned} \tag{71}$$

By taking these expressions, for the derivative of the current through the inductor and the voltage over the capacitor, it is now possible to build the A matrix:

$$\mathbf{A_1} = \begin{bmatrix} -\frac{R_tN^2 + \frac{R_cR_o}{(R_o+R_c)}}{LN^2} & \frac{R_o}{NL(R_o+R_c)} \\ -\frac{R_o}{CN(R_o+R_c)} & -\frac{1}{C(R_o+R_c)} \end{bmatrix} \tag{72}$$

The **B** matrix is in this case equal to:

$$\mathbf{B_1} = \begin{bmatrix} \frac{1}{L} \\ 0 \end{bmatrix} \tag{73}$$

This A matrix and the above described derivation process pertain to **the first state** of the converter, from time = t_0 until time = t_1. In this first state it is the switches S1, S4 - on the primary, and S6, S7 - on the secondary side, that conduct the current.

The four states of the converter are clearly discernible in figure 7.

In the second state, between t_1 and t_2, it is the switches S1, S4 and S5, S8 that conduct the current on the primary and secondary sides, respectively. The circuit diagram that corresponds to this second state is depicted below, in figure 22:

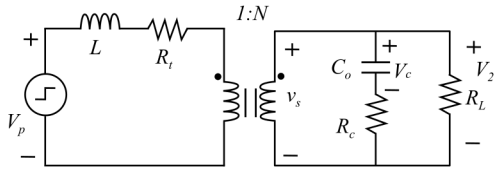

Figure 22: DAB converter in the 2^{nd} state

As before, the presence of the HFT implies that $v_p = \frac{v_s}{N}$ and $i_{L2} = \frac{i_L}{N}$. Starting out once again with KVL:

$$
\begin{aligned}
&\begin{cases} V_L = v_p - V_{R_t} - \dfrac{v_s}{N} \\ v_s = V_c + i_c R_c \end{cases} \implies \\
&V_L = v_p - i_L R_t - (\frac{V_c + i_c R_c}{N}) = v_p - i_L R_T - \frac{V_c}{N} - \frac{i_c R_c}{N} \Leftrightarrow \\
&L\frac{di_L}{dt} = v_p - i_L R_t - \frac{V_c}{N} - \frac{R_c}{N} C\frac{dV_c}{dt} \Leftrightarrow \\
&\frac{di_L}{dt} = \frac{v_p}{L} - i_L\frac{R_t}{L} - \frac{V_c}{LN} - \frac{CR_c}{LN}\frac{dV_c}{dt}
\end{aligned}
\tag{74}
$$

Next, we find the expression for the current through the capacitor:

$$
\begin{aligned}
&i_{L2} = i_c + i_o \implies i_c = i_{L2} - i_o \\
&\textit{but } i_{L2} = \frac{i_L}{N} \implies i_c = \frac{1}{N} i_L - i_o \\
&\textit{and } i_o = \frac{V_2}{R_o} = \frac{V_c + V_{R_c}}{R_o} = \frac{V_c}{R_o} + \frac{i_c R_c}{R_o} \\
&\textit{such that } i_c = \frac{1}{N} i_L - \frac{V_c}{R_o} - \frac{i_c R_c}{R_o} \implies \\
&i_c + \frac{i_c R_c}{R_o} = \frac{1}{N} i_L - \frac{V_c}{R_o} \Leftrightarrow \\
&i_c(\frac{R_o + R_c}{R_o}) = \frac{1}{N} i_L - \frac{V_c}{R_o} \implies \\
&i_c = \frac{1}{N} i_L \frac{R_o}{(R_o + R_c)} - V_c \frac{1}{(R_o + R_c)} \Leftrightarrow \\
&C\frac{dV_c}{dt} = i_L \frac{R_o}{N(R_o + R_c)} - V_c \frac{1}{(R_o + R_c)} \implies \\
&\boxed{\frac{dV_c}{dt} = i_L \frac{R_o}{NC(R_o + R_c)} - V_c \frac{1}{C(R_o + R_c)}}
\end{aligned}
\tag{75}
$$

Now, the expression developed for the capacitor current is inserted into the equation defining the voltage over the inductor:

$$\begin{aligned}\frac{di_L}{dt} &= \frac{v_p}{L} - i_L\frac{R_t}{L} - \frac{V_c}{LN} - \frac{CR_c}{LN}(i_L\frac{R_o}{NC(R_o+R_c)} - V_c\frac{1}{C(R_o+R_c)}) \\ &= \frac{v_p}{L} - i_L\frac{R_t}{L} - \frac{V_c}{LN} - i_L\frac{R_oR_c}{LN^2(R_o+R_c)} + V_c\frac{R_c}{LN(R_o+R_c)}) \\ &= \frac{v_p}{L} - i_L(\frac{R_t}{L} + \frac{R_oR_c}{LN^2(R_o+R_c)}) - V_c(\frac{1}{LN} - \frac{R_c}{LN(R_o+R_c)}) \\ &= \frac{v_p}{L} - i_L\frac{R_tLN^2(R_+R_c) + R_oR_cL}{L^2N^2(R_o+R_c)} - V_c\frac{LN(R_o+R_c) - LNR_c}{L^2N^2(R_o+R_c)} \\ \boxed{\frac{di_L}{dt} &= \frac{v_p}{L} - i_L\frac{R_tN^2 + \frac{R_oR_c}{R_o+R_c}}{LN^2} - V_c\frac{R_o}{LN(R_o+R_c)}}\end{aligned} \tag{76}$$

And the expressions derived above yield the following A matrix describing the second state of the converter:

$$\mathbf{A_2} = \begin{bmatrix} -\frac{N^2R_t + \frac{R_oR_c}{R_o+R_c}}{N^2L} & \frac{R_o}{NL(R_o+R_c)} \\ \frac{R_o}{NC(R_o+R_c)} & -\frac{1}{C(R_o+R_c)} \end{bmatrix} \tag{77}$$

And the $\mathbf{B}$ matrix is in this second identical to the one in the first state

$$\mathbf{B_2} = \begin{bmatrix} \frac{1}{L} \\ 0 \end{bmatrix} \tag{78}$$

It has been pointed out before that the first and fourth state have identical circuit diagrams, as do the second and third state, see figures 11, 12, 13 and 14.

This allows us to write that $\mathbf{A_1} = \mathbf{A_4}$ and $\mathbf{A_2} = \mathbf{A_3}$. Regarding the $\mathbf{B}$ matrices of the four states, it can be established by observation that $\mathbf{B_1} = \mathbf{B_2}$ and $\mathbf{B_3} = \mathbf{B_4}$.

Summing up the analysis that has been done so far on the DAB converter under SPS modulation:

$$\mathbf{A_1} = \mathbf{A_4} = \begin{bmatrix} -\dfrac{R_t N^2 + \dfrac{R_c R_o}{R_o + R_c}}{LN^2} & \dfrac{R_o}{NL(R_o + R_c)} \\ -\dfrac{R_o}{CN(R_o + R_c)} & -\dfrac{1}{C(R_o + R_c)} \end{bmatrix} \tag{79}$$

$$\mathbf{A_2} = \mathbf{A_3} = \begin{bmatrix} -\dfrac{N^2 R_t + \dfrac{R_o R_c}{R_o + R_c}}{N^2 L} & \dfrac{R_o}{NL(R_o + R_c)} \\ \dfrac{R_o}{NC(R_o + R_c)} & -\dfrac{1}{C(R_o + R_c)} \end{bmatrix} \tag{80}$$

$$\mathbf{B_1} = \mathbf{B_2} = \begin{bmatrix} \dfrac{1}{L} \\ 0 \end{bmatrix} \tag{81}$$

$$\mathbf{B_3} = \mathbf{B_4} = \begin{bmatrix} -\dfrac{1}{L} \\ 0 \end{bmatrix} \tag{82}$$

Obtaining the state matrices concludes the first part of the model derivation. The second part of the process builds on the observation that state variable values of one state are based on initial conditions, which are in fact the values of the state variable of the previous state. It can be written that

- the values of the state variables of the first state, are determined by the initial values of the state variables, which coincide with the state variable values of the last state of the previous switching cycle

$$\mathbf{x}_{n1} = f_{tn1}(\mathbf{x}_n, \phi_n) = e^{\mathbf{A_1} t_{n1}} \mathbf{x}_n + \Psi_1 V_1 \tag{83}$$

- when computing the values of the state variables of the second state, $\mathbf{x}_{n2}$ it is the values of the first state that are taken to be the initial conditions

$$\mathbf{x}_{n2} = f_{tn2}(\mathbf{x}_{n1}, \phi_n) = e^{\mathbf{A_2} t_{n2}} \mathbf{x}_{n1} + \Psi_2 V_1 \tag{84}$$

- similarly, when computing the values of the state variables of the third state, $\mathbf{x}_{n3}$, the end values of the state variables pertaining to the second state serve as the initial values

$$\mathbf{x}_{n3} = f_{tn3}(\mathbf{x}_{n2}, \phi_n) = e^{\mathbf{A_3} t_{n3}} \mathbf{x}_{n2} + \Psi_3 V_1 \tag{85}$$

- the values of the state variables of the fourth state, the same as the initial conditions of the next switching cycle $\mathbf{x}_{n+1} = \mathbf{x}_{n4}$ are determined by the state variable values

of the previous state

$$\mathbf{x}_{n+1} = f_{tn4}(\mathbf{x}_{n3}, \phi_n) = e^{\mathbf{A_4} t_{n4}} \mathbf{x}_{n3} + \Psi_4 V_1 \tag{86}$$

where:

$$\begin{aligned}
\mathbf{\Psi_1} &= \int_0^{t_1} e^{\mathbf{A_1}\tau} \mathbf{B_1} d\tau = \mathbf{A_1}^{-1} [e^{\mathbf{A_1}\tau}]_0^{t_{t_{n1}}} \mathbf{B_1} \\
&= \mathbf{A_1}^{-1} (e^{\mathbf{A_1} t_{n1}} - I) \mathbf{B_1} \\
\mathbf{\Psi_2} &= \int_0^{t_2} e^{\mathbf{A_2}\tau} \mathbf{B_2} d\tau = \mathbf{A_2}^{-1} [e^{\mathbf{A_2}\tau}]_0^{t_{n2}} \mathbf{B_2} \\
&= \mathbf{A_2}^{-1} (e^{\mathbf{A_2} t_{n2}} - I) \mathbf{B_2} \\
\mathbf{\Psi_3} &= \int_0^{t_3} e^{\mathbf{A_3}\tau} \mathbf{B_3} d\tau = \mathbf{A_3}^{-1} [e^{\mathbf{A_3}\tau}]_0^{t_{n3}} \mathbf{B_3} \\
&= \mathbf{A_3}^{-1} (e^{\mathbf{A_3} t_{n3}} - I) \mathbf{B_3} \\
\mathbf{\Psi_4} &= \int_0^{t_4} e^{\mathbf{A_4}\tau} \mathbf{B_4} d\tau = \mathbf{A_4}^{-1} [e^{\mathbf{A_4}\tau}]_0^{t_{n4}} \mathbf{B_4} \\
&= \mathbf{A_4}^{-1} (e^{\mathbf{A_4} t_{n4}} - I) \mathbf{B_4}
\end{aligned} \tag{87}$$

$\phi_n \in [0,\pi]$ is the phase shift of the *nth* cycle, and t_{n1}, t_{n2}, t_{n3} and t_{n4} denote the time intervals of the states 1 to 4, respectively. Mathematically these intervals are expressed as:

$$\begin{aligned}
t_{n1} = t_{n3} &= \frac{\phi_n}{2\pi f_s} \\
t_{n2} = t_{n4} &= \frac{1}{2 f_s} - \frac{\phi_n}{2\pi f_s}
\end{aligned} \tag{88}$$

As in the previously presented case of the buck converter, it is therefore possible to write that

$$\mathbf{x}_{n+1} = \mathbf{F}(\phi_n)\mathbf{x}_n + \mathbf{G}(\phi_n) V_1 \tag{89}$$

where

$$\mathbf{F}(\phi_n) = e^{\mathbf{A_4} t_{n4}} e^{\mathbf{A_3} t_{n3}} e^{\mathbf{A_2} t_{n2}} e^{\mathbf{A_1} t_{n1}} \tag{90}$$

and

$$\mathbf{G}(\phi_n) = e^{\mathbf{A_4} t_{n4}} e^{\mathbf{A_3} t_{n3}} e^{\mathbf{A_2} t_{n2}} \Psi_1 + e^{\mathbf{A_4} t_{n4}} e^{\mathbf{A_3} t_{n3}} \Psi_2 + e^{\mathbf{A_4} t_{n4}} \Psi_3 + \Psi_4 \tag{91}$$

Put clearly, the above expressions can intuitively be rewritten as

$$\begin{aligned}\mathbf{x}_{n+1} &= f_{tn4}(f_{tn3}(f_{tn2}(f_{tn1}(\mathbf{x}_n, \phi_n)))) \\ &= e^{\mathbf{A_4}t_{n4}}(e^{\mathbf{A_3}t_{n3}}(e^{\mathbf{A_2}t_{n2}}(e^{\mathbf{A_1}t_{n1}}\mathbf{x}_n + \mathbf{\Psi_1}\mathbf{V_1}) + \mathbf{\Psi_2}V_1) + \mathbf{\Psi_3}V_1) + \mathbf{\Psi_4}V_1\end{aligned} \tag{92}$$

By observing the expressions presented above, it is easy to notice that the matrix exponential plays an important role. While finding the value of this expression is usually done with the help of a computer and engineering software, such as MATLAB, it can also be done in different ways:

1. use the Laplace transform, if we are using continuous-time model
2. use the Z transform if we are using the DT model
3. use "the straight line" approximation, obtained from the Taylor series, which is sufficiently accurate and simple to calculate [9]

Yet another method, presented in [21], is the bilinear approximation method, by which the matrix exponentials are approximated by expanding them around the steady-state operation phase shift:

$$\begin{aligned}
e^{\mathbf{A_1}t_{n1}} &= e^{\mathbf{A_1}T_\phi}e^{\mathbf{A_1}(t_{n1}-T_\phi)} \approx e^{\mathbf{A_1}T_\phi}(\mathbf{I} + \mathbf{A_1}(t_{n1} - T_\phi)) \\
e^{\mathbf{A_2}t_{n2}} &= e^{\mathbf{A_2}(\frac{T_s}{2}-T_\phi)}e^{\mathbf{A_2}(t_{n2}-\frac{T_s}{2}+T_\phi)} \approx e^{\mathbf{A_2}(\frac{T_s}{2}-T_\phi)}(\mathbf{I} + \mathbf{A_2}(t_{n2} - \frac{T_s}{2} + T_\phi)) \\
e^{\mathbf{A_3}t_{n3}} &= e^{\mathbf{A_3}T_\phi}e^{\mathbf{A_3}(t_{n3}-T_\phi)} \approx e^{\mathbf{A_3}T_\phi}(\mathbf{I} + \mathbf{A_3}(t_{n3} - T_\phi)) \\
e^{\mathbf{A_4}t_{n4}} &= e^{\mathbf{A_4}(\frac{T_s}{2}-T_\phi)}e^{\mathbf{A_4}(t_{n4}-\frac{T_s}{2}+T_\phi)} \approx e^{\mathbf{A_4}(\frac{T_s}{2}-T_\phi)}(\mathbf{I} + \mathbf{A_4}(t_{n4} - \frac{T_s}{2} + T_\phi))
\end{aligned} \tag{93}$$

where ϕ is the steady-state phase shift, and $T_\phi = \frac{\phi}{2\pi f_s}$.

One major advantage of the bilinear approximation is that the matrix exponentials of the resulting expressions do not contain any control variables, and as such they can be treated as constants, being computed in advance, and thus substantially reducing the computation necessities in the case of complex systems.

It must be pointed out at this point that as in the case of the buck converter, the only varying variables in the expressions presented above are the time intervals, which in their turn depend on the phase shift, ϕ. Computing this input (control) parameter depends on the control strategy that has been chosen. As the choice of an optimal control technique can be a complex task, it is outside the scope of the present paper. However, drawing once again on the similarities with the aforementioned model of the Buck converter, it is here presumed that a simple proportional controller is employed. The resulting expression for the phase shift value is:

$$\phi_{n+1} = k(V_{ref,n} - V_{2n}) \tag{94}$$

where k is the gain of the proportional controller, and $\phi_{n+1} \in [0, \frac{\pi}{2}]$.

Just as in the analysis of the Buck converter, the voltage over the load, V_2 can be expressed in the form of a sum between the voltage over the capacitor, and the voltage over the capacitor ESR. V_2 is equal to the product of the $\mathbf{C}$ matrix and the column vector of the state variables. Keeping in mind that the four states of the converter can be described by only two circuit diagrams, and $\mathbf{A_1} = \mathbf{A_4}$ and $\mathbf{A_2} = \mathbf{A_3}$, it is expected that there are at most two distinct $\mathbf{C}$ matrices.

Referring to the circuit diagram depicting **the first and fourth states**, figure 11, the following can be stated:

$$\begin{aligned}
&\begin{cases} V_2 = V_c + i_c R_c \\ i_c = -i_L \dfrac{R_L}{R_L + R_c} - V_c \dfrac{1}{R_L + R_c} \end{cases} \implies \\
V_2 &= V_c - i_L \frac{R_L R_c}{R_L + R_c} - V_c \frac{R_c}{R_L + R_c} \\
&= -i_L \frac{R_L R_c}{R_L + R_c} + V_c (1 - \frac{R_c}{R_L + R_c}) \\
&= -i_L \frac{R_L R_c}{R_L + R_c} + V_c \frac{R_L}{R_L + R_c}
\end{aligned} \tag{95}$$

Next, by observing the equivalent circuit diagram of **the second and third states**, figure 12, the following mathematical expression holds true:

$$\begin{aligned}
&\begin{cases} V_2 = V_c + i_c R_c \\ i_c = i_L \dfrac{R_L}{R_L + R_c} - V_c \dfrac{1}{R_L + R_c} \end{cases} \implies \\
V_2 &= V_c + i_L \frac{R_L R_c}{R_L + R_c} - V_c \frac{R_c}{R_L + R_c} \\
&= i_L \frac{R_L R_c}{R_L + R_c} + V_c (1 - \frac{R_c}{R_L + R_c}) \\
&= i_L \frac{R_L R_c}{R_L + R_c} + V_c \frac{R_L}{R_L + R_c}
\end{aligned} \tag{96}$$

The calculations conducted above yielded the complete form of the output voltage, but by composing the $\mathbf{C}$ matrices it becomes clear that similar to the Buck converter, also here the two matrices are identical, and it is thus sufficient to write that:

$$\mathbf{C} = \begin{bmatrix} -\dfrac{R_L R_c}{R_L + R_c} \\ \dfrac{R_L}{R_L + R_c} \end{bmatrix} \tag{97}$$

The next task is to test for the stability of the system. This check is performed exactly like in the case of the Buck converter: by composing the Jacobian, finding its eigenvalues

and comparing their absolute values to 1. This is the structure of the Jacobian:

$$J(I_L, V_c, \Phi) = \begin{bmatrix} \frac{\partial i_{L(n+1)}}{\partial i_{Ln}} & \frac{\partial i_{L(n+1)}}{\partial v_{cn}} & \frac{\partial i_{L(n+1)}}{\partial \phi_n} \\ \frac{\partial v_{c(n+1)}}{\partial i_{Ln}} & \frac{\partial v_{c(n+1)}}{\partial v_{cn}} & \frac{\partial v_{c(n+1)}}{\partial \phi_n} \\ \frac{\partial \phi_{(n+1)}}{\partial i_{Ln}} & \frac{\partial \phi_{(n+1)}}{\partial v_{cn}} & \frac{\partial \phi_{(n+1)}}{\partial \phi_n} \end{bmatrix} \tag{98}$$

The eigenvalues are found by solving the following equation:

$$det(\lambda I - J(I_L, V_c, D)) = 0 \tag{99}$$

3.3.3 The DAB converter model under EPS modulation

Based on the diagram of the DAB converter under EPS operation depicted above in figure 8, it is possible to draw the circuit diagrams for each of the six states of the DAB converter under EPS.

Starting off with the period between t_0 and t_1, the circuit diagram for **the first state** is depicted below:

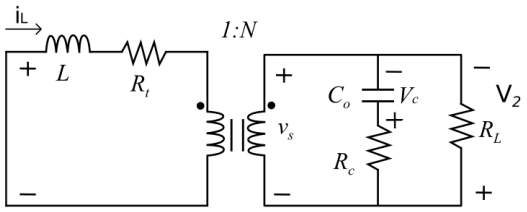

Figure 23: DAB converter circuit diagram representing the first state

Given that there is no input voltage source present in this state, this circuit is similar, and indeed can be reduced to the equivalent circuit of a Buck converter when the switch is in the OFF position. The corresponding equations are derived below, by use of the loop current circuit analysis technique. From the first loop we obtain that:

$$\begin{aligned} &i_L R_t + V_L - V_c + R_c(i_L - i_o) = 0 \Leftrightarrow \\ &i_L R_t + V_L - V_c + R_c(i_L - i_L - i_c)) = 0 \Leftrightarrow \\ &i_L R_t + V_L - V_c - R_c i_c = 0 \Leftrightarrow \\ &V_L = R_c i_c + V_c - R_t i_L \end{aligned} \tag{100}$$

Then, the expression for i_c is obtained from the second loop:

$$\begin{aligned}
&V_c + R_o i_o + R_c(i_o - i_L) = 0 \Leftrightarrow \\
&V_c + R_o i_o + R_c i_o - R_c i_L = 0 \Leftrightarrow \\
&V_c + i_o(R_o + R_c) - R_c i_L = 0 \Leftrightarrow \\
&V_c + (R_o + R_c)(i_L + i_c) - R_c i_L = 0 \Leftrightarrow \\
&V_c + R_o i_L + R_o i_c + R_c i_L + R_c i_c - R_c i_L = 0 \Leftrightarrow \\
&V_c + R_o i_L + i_c(R_o + R_c) = 0 \implies \\
&i_c = -i_L \frac{R_o}{R_o + R_c} - V_c \frac{1}{R_o + R_c}
\end{aligned} \tag{101}$$

and inserting this expression for i_c in the equation for the inductor voltage yields that:

$$\begin{aligned}
V_L &= V_c - i_L R_t + R_c(-i_L \frac{R_o}{R_o + R_c} - V_c \frac{1}{R_o + R_c}) \\
&= V_c - i_L R_t - i_L \frac{R_c R_o}{R_o + R_c} - V_c \frac{R_c}{R_o + R_c}) \\
&= i_L(-R_t - \frac{R_c R_o}{R_o + R_c}) + V_c(1 - \frac{R_c}{R_o + R_c}) \\
&= i_L(-R_t - \frac{R_c R_o}{R_o + R_c}) + V_c \frac{R_o + R_c - R_c}{R_o + R_c} \\
&= i_L(-R_t - \frac{R_c R_o}{R_o + R_c}) + V_c \frac{R_o}{R_o + R_c} \\
\frac{di_L}{dt} &= i_L(-\frac{R_t}{L} - \frac{R_c R_o}{L(R_o + R_c)}) + V_c \frac{R_o}{L(R_o + R_c)}
\end{aligned} \tag{102}$$

and by remembering to refer the inductor current and the copper resistance of the primary to the secondary side, the exact same expressions are obtained as the ones describing the first state of the DAB converter under SPS modulation:

$$\boxed{\begin{aligned}
\frac{di_L}{dt} &= -i_L \frac{R_t N^2 + \dfrac{R_c R_o}{(R_o + R_c)}}{L^2 N^2} + V_c \frac{R_o}{NL(R_o + R_c)} \\
\frac{dV_c}{dt} &= -i_L \frac{R_o i_L}{NC(R_o + R_c)} - V_c \frac{1}{C(R_o + R_c)}
\end{aligned}} \tag{103}$$

The circuit diagram of **the second state**, between t_1 and t_2 is presented below:

This circuit diagram is identical to that representing the first state of the DAB converter under SPS modulation, see figure 11, and thus it will be expressed by the same mathematical expressions(72, 73) .

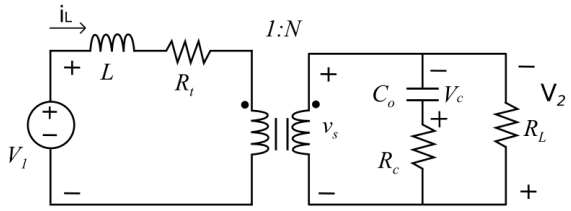

Figure 24: DAB converter circuit diagram representing the second state

The third state, between t_2 and t_3 is represented by the following circuit diagram:

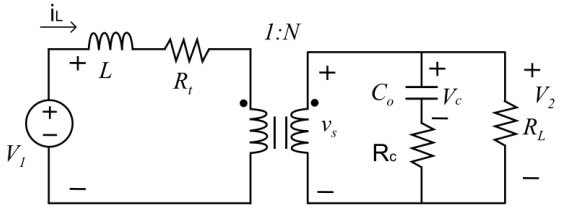

Figure 25: DAB converter circuit diagram representing the third state

It must be noted that this circuit diagram is identical to the one describing the second state of the DAB converter under SPS operation, see figure 12, and thus it will be expressed by the same mathematical expressions (77, 78) .

The circuit diagram pertaining to **the fourth state** of the DAB converter, under EPS modulation is depicted below in figure 26.

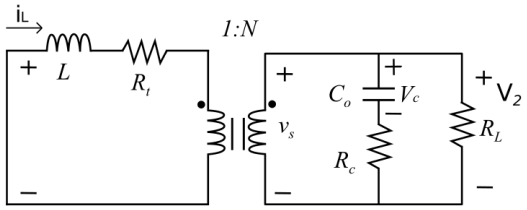

Figure 26: DAB converter circuit diagram representing the fourth state

The fact that there is no voltage source connected on the primary side suggests that also the circuit diagram of this state is similar to that of a Buck converter when the switch is open.

From the first loop we obtain that:

$$\begin{aligned} &i_L R_t + V_L + V_c + R_c(i_L - i_o) = 0 \Leftrightarrow \\ &i_L R_t + V_L + V_c + R_c(i_L - i_L - i_c)) = 0 \Leftrightarrow \\ &i_L R_t + V_L + V_c - R_c i_c = 0 \Leftrightarrow \\ &V_L = R_c i_c - V_c - R_t i_L \end{aligned} \tag{104}$$

Then, the expression for i_c is obtained from the second loop:

$$\begin{aligned} &R_o i_o + R_c(i_o - i_L) - V_c = 0 \Leftrightarrow \\ &R_o i_o + R_c i_o - R_c i_L - V_c = 0 \Leftrightarrow \\ &i_o(R_o + R_c) - R_c i_L - V_c = 0 \Leftrightarrow \\ &(R_o + R_c)(i_L - i_c) - R_c i_L - V_c = 0 \Leftrightarrow \\ &R_o i_L - R_o i_c + R_c i_L - R_c i_c - R_c i_L - V_c = 0 \Leftrightarrow \\ &R_o i_L - i_c(R_o + R_c) - V_c = 0 \implies \\ &i_c = i_L \frac{R_o}{R_o + R_c} - V_c \frac{1}{R_o + R_c} \end{aligned} \tag{105}$$

and inserting this expression for i_c in the equation for the inductor voltage yields that:

$$\begin{aligned} V_L &= -i_L R_t - V_c - R_c(i_L \frac{R_o}{R_o + R_c} - V_c \frac{1}{R_o + R_c}) \\ &= -i_L R_t - V_c - i_L \frac{R_c R_o}{R_o + R_c} + V_c \frac{R_c}{R_o + R_c}) \\ &= i_L(-R_t - \frac{R_c R_o}{R_o + R_c}) + V_c(-1 + \frac{R_c}{R_o + R_c}) \\ &= i_L(-R_t - \frac{R_c R_o}{R_o + R_c}) - V_c \frac{R_o}{R_o + R_c} \\ \frac{di_L}{dt} &= i_L(-\frac{R_t}{L} - \frac{R_c R_o}{L(R_o + R_c)}) - V_c \frac{R_o}{L(R_o + R_c)} \end{aligned} \tag{106}$$

and by remembering to refer the inductor current and the copper resistance of the primary to the secondary side, the exact same expressions are obtained as the ones describing the first state of the DAB converter under SPS modulation:

$$\boxed{\begin{aligned} \frac{di_L}{dt} &= -i_L \frac{R_t N^2 + \frac{R_c R_o}{(R_o + R_c)}}{L^2 N^2} - V_c \frac{R_o}{NL(R_o + R_c)} \\ \frac{dV_c}{dt} &= i_L \frac{R_o i_L}{NC(R_o + R_c)} - \frac{V_c}{C(R_o + R_c)} \end{aligned}} \tag{107}$$

Spanning the time period between t_4 and t_5, **the fifth state** of the DAB converter is described by the following circuit diagram:

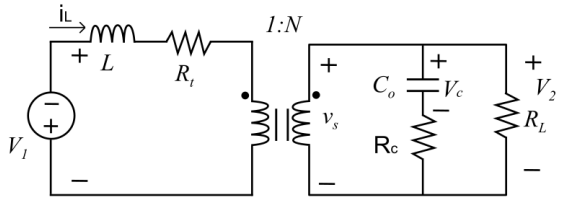

Figure 27: DAB converter circuit diagram representing the fifth state

Upon careful observation, it becomes evident that the circuit diagram of this state is identical with the one pertaining to the third state of the DAB converter under SPS modulation, see figure 13, and is therefore characterised by the same mathematical expressions (77, 78).

The sixth and final state, between t_5 and t_6 is described by the following circuit diagram:

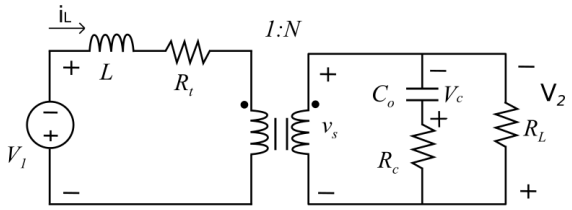

Figure 28: DAB converter circuit diagram representing the sixth state

As in the case of the previous states that include the input voltage source, this final state of the switching cycle is represented by a circuit diagram identical with the one corresponding to the fourth state of the DAB converter under SPS modulation, see figure 14, and is therefore characterised by the same mathematical expressions (72, 73).

In conclusion, it can be stated that the six states of the DAB converter under EPS modulation are bear strong similarities to those observed under SPS modulation. When composing the **A**, **B**, and **C** matrices, one notices the following relationships:

Table 2: Similarities of the DAB converter state matrices under SPS and EPS modulation

A MATRICES	B MATRICES
$\mathbf{A_{1_{EPS}}} = \mathbf{A_{1_{SPS}}} = \mathbf{A_{4_{SPS}}}$	$\mathbf{B_{1_{EPS}}} = \mathbf{0}$
$\mathbf{A_{2_{EPS}}} = \mathbf{A_{1_{SPS}}} = \mathbf{A_{4_{SPS}}}$	$\mathbf{B_{2_{EPS}}} = \mathbf{B_{1_{SPS}}} = \mathbf{B_{2_{SPS}}}$
$\mathbf{A_{3_{EPS}}} = \mathbf{A_{2_{SPS}}} = \mathbf{A_{3_{SPS}}}$	$\mathbf{B_{3_{EPS}}} = \mathbf{B_{2_{SPS}}} = \mathbf{B_{1_{SPS}}}$
$\mathbf{A_{4_{EPS}}} = \mathbf{A_{3_{SPS}}} = \mathbf{A_{2_{SPS}}}$	$\mathbf{B_{4_{EPS}}} = \mathbf{0}$
$\mathbf{A_{5_{EPS}}} = \mathbf{A_{3_{SPS}}} = \mathbf{A_{2_{SPS}}}$	$\mathbf{B_{5_{EPS}}} = \mathbf{B_{3_{SPS}}} = \mathbf{B_{4_{SPS}}}$
$\mathbf{A_{6_{EPS}}} = \mathbf{A_{4_{SPS}}} = \mathbf{A_{1_{SPS}}}$	$\mathbf{B_{6_{EPS}}} = \mathbf{B_{4_{SPS}}} = \mathbf{B_{3_{SPS}}}$

Also the $\mathbf{C}$ matrix of the DAB under EPS must then be identical to the one obtained under SPS modulation.

The stability analysis is carried out in the same way as under SPS, and is therefore not reproduced here.

4 Chapter 4 - Numerical example and discussion

The purpose of this chapter is to test the discrete time model that has been laid out in chapter 3, and to comment on the results. The Buck converter has been used as a support tool during the writing of this thesis. It aided in understanding the mechanics of the DAB converter, the setup of the discrete model. In this chapter, the Buck converter is again employed to validate the accuracy of the conventional approximation to obtain the values of the matrix exponential, as well as the stability considerations of switching converters in general. Despite of its simpler structure, it provides sufficiently complex to demonstrate the simple proportional control and the effect of the proportional gain on the converter on the stability of the system.

The ensuing validation of the DAB converter is restricted to verifying the accuracy of the model under steady state operation. For obtaining the simulation data and compose the combined plots of the simulation and the discrete model, the circuits were constructed in PLECS, and then exported to MATLAB's workspace by way of the ingenious interaction between the two software toolboxes. PLECS has been found to be a simple, fast and powerful design software tool.

4.1 Validating the model of the Buck converter

The model of the Buck converter is validated first by comparing it to a model constructed in Simulink.

The numerical values of the Buck converter are displayed in the tables below:

Table 3: Buck converter parameter values

V_1 [V]	R_t [Ω]	L [H]	C [F]	R_c [Ω]	R_o [Ω]	f_s [Hz]	T_s [s]
500	0.02	1.2e-3	100e-6	1e-3	5	25e3	4e-5

The first two images present the steady state operating point of the Buck converter, as obtained by simulation, as well as using the discrete time model presented in chapter 3, with two different versions of calculating the matrix exponentials:

- one version where the matrix exponentials are calculated by the internal algorithm of MATLAB
- and one version where the matrix exponentials are obtained using the conventional approximation - the first order term of the Taylor series expansion

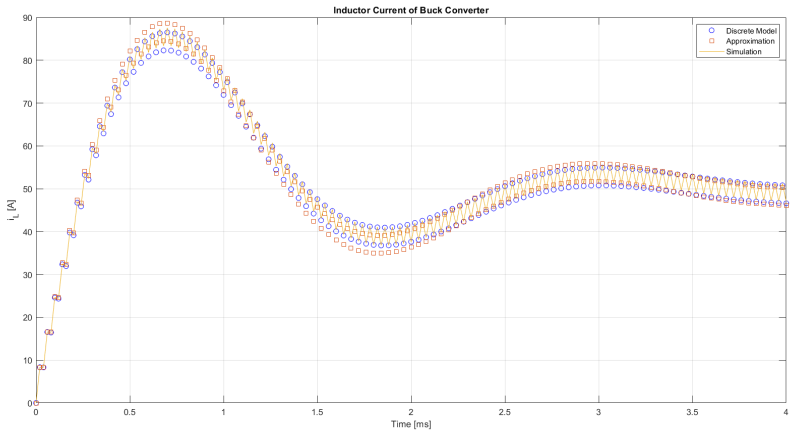

(a) steady state i_L waveforms

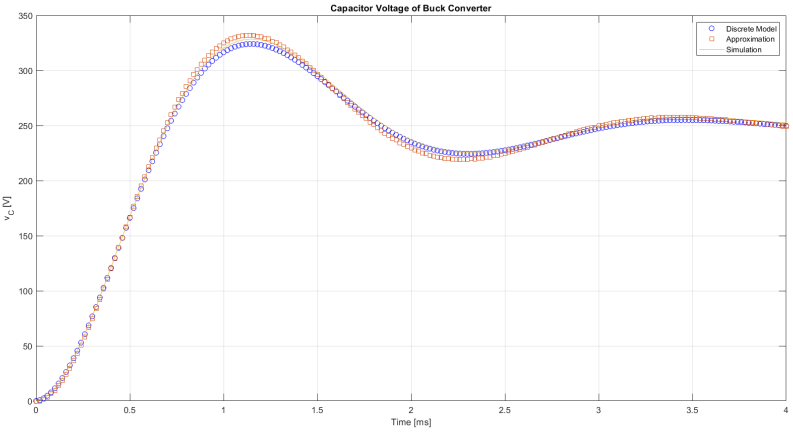

(b) steady state V_c waveforms

As it can be seen in the pictures above, the model is close to the actual simulation, following it through the transients, until the system reaches steady state. The converter values are as expected.

To next set of images offer a provide a closer look at the i_L and V_c waveforms during the transient period, and two close up diagrams presenting the settled, steady state waveforms:

It can be noted that once the system has achieved steady state, the approximation of the matrix exponential yields an equivalent result to the MATLAB algorithm.

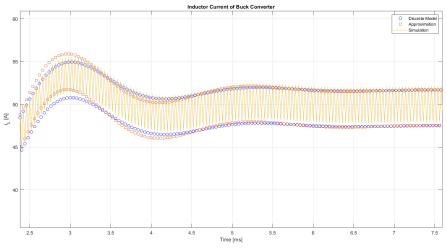

(a) i_L transient waveforms

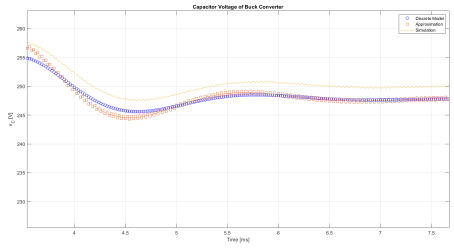

(b) V_c transient waveforms

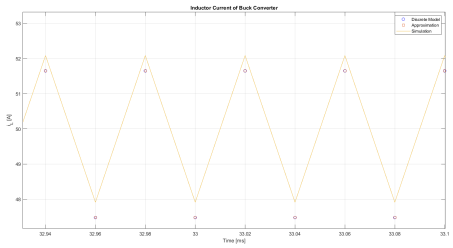

(c) i_L steady state waveforms

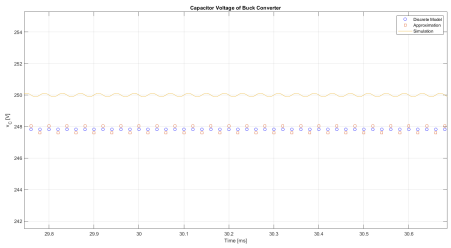

(d) V_c steady state waveforms

Next, the results of the stability analysis are shown below. As previously mentioned in chapter 3, in addition to assessing the stability by obtaining the eigenvalues of the Jacobian, and calculating their absolute value, which is then compared to 1, there is also an alternative method. By plotting a range of values of the proportional gain k against the values of the inductor current, it is possible to observe any bifurcations that may arise. The next plot shows the bifurcation diagram:

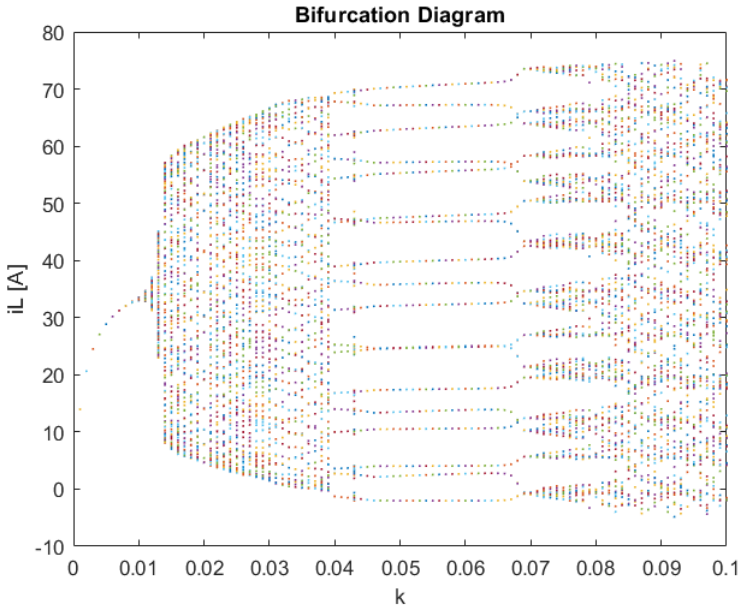

Figure 31: Buck converter bifurcation diagram

As it can be observed from the bifurcation diagram, the system loses its 1 period stability

rather quickly, for rather small values of k. It must therefore be noted at this point that some of the system parameters would probably need modifying in a real life situation, as the speed of the regulator is directly proportional with the value of the proportional gain. Put in a nutshell, the higher the k value that can be used, the faster the response of the system.

To illustrate the inefficiency of a small gain value, the next image shows the inductor current and capacitor voltage when steady state is reached, with a k value of 6e-3. The reader is now reminded that steady state does not imply zero steady state error.

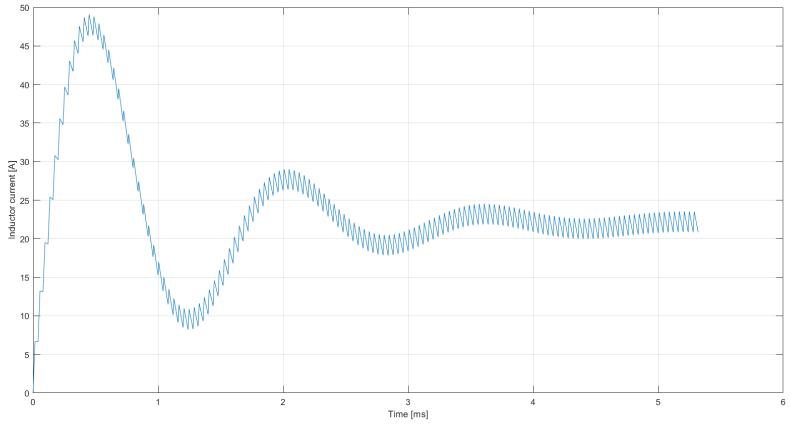

(a) period 1 steady state i_L waveform

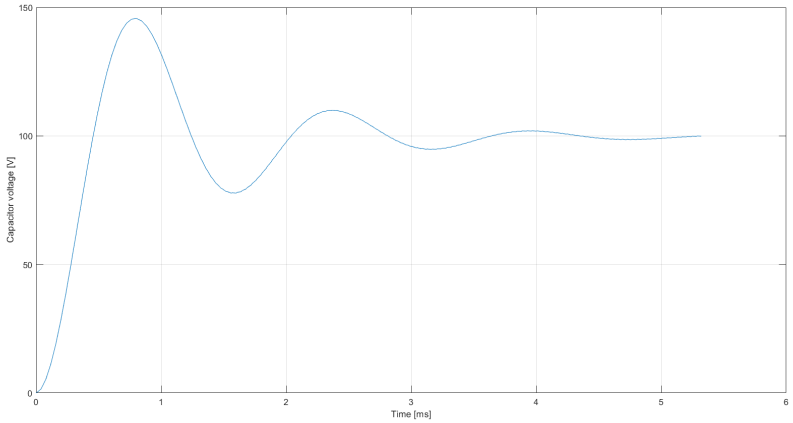

(b) period 1 steady state V_c waveform

The steady state error of the capacitor voltage is around 150 V. However, it is in this case more important to focus on the equilibrium attractor that the system will gravitate towards, given a certain value of the controller gain, when all other system parameters remain unchanged.

In the case of the diagrams depicting the steady state of the converter included above, figures 29a and 29b, the proportional control was not implemented, and the feedback loop was not in place. However, it was observed that zero steady state error stability was

attained for a value of $k = 0.11$. The crucial difference, however, is that observing the bifurcation diagram, one will notice that this was a random steady state obtained from an infinite pile of steady states, with no periodicity or predictability.

4.2 Validating the model of the DAB converter

The model of the DAB converter is validated first by comparing it to a model constructed in Simulink.

The numerical values of the Buck converter are displayed in the tables below:

Table 4: DAB converter parameter values

V_1 [V]	R_t [Ω]	L [H]	C [F]	R_c [Ω]	R_o [Ω]	f_s [Hz]	T_s [s]	D	N
700	0.02	6.125e-6	25e-6	1e-3	4.9	100e3	1e-5	0.5	1

Just as in the preceding case of the Buck converter, the goal is to verify the validity of the discrete model, when compared with an actual Simulink simulation. Based on the numerical values from table 4, the following diagrams are obtained for the steady state operation **under SPS**:

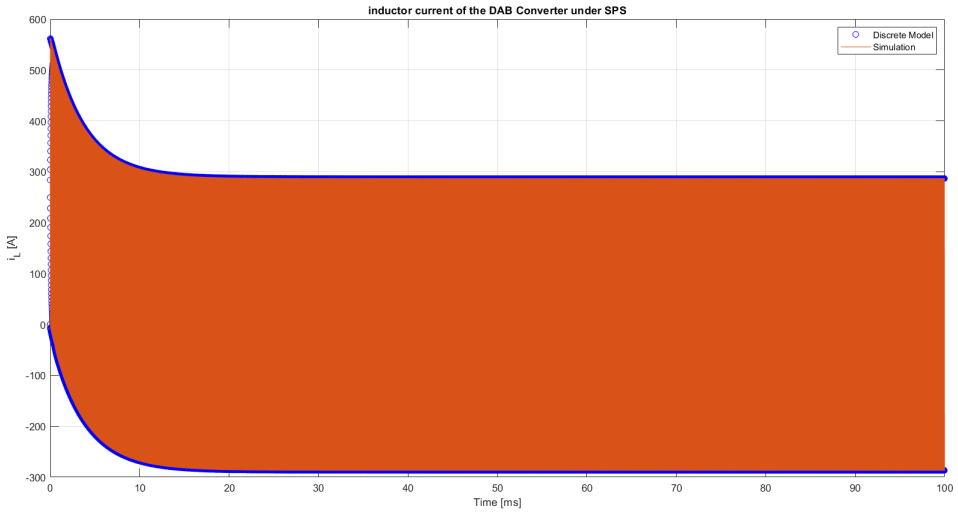

Figure 33: the inductor current of the DAB converter under SPS

The figure shows that the model follows the simulation perfectly. The following figure provides the reader with a closer look at the waveform of i_L under SPS, confirming the accuracy of the model:

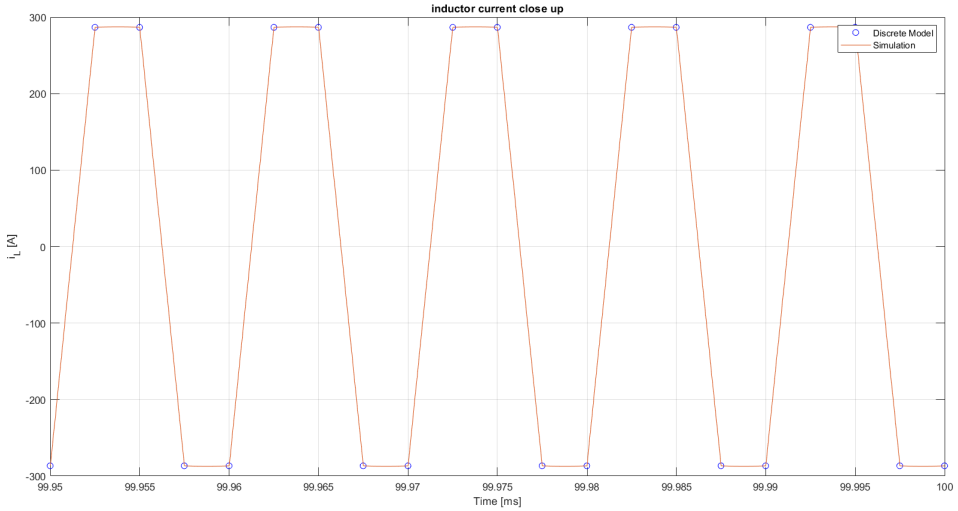

Figure 34: close caption of the waveform of the inductor current under SPS

The steady state waveform of the voltage over the output capacitor of the DAB converter, under SPS modulation, is presented next:

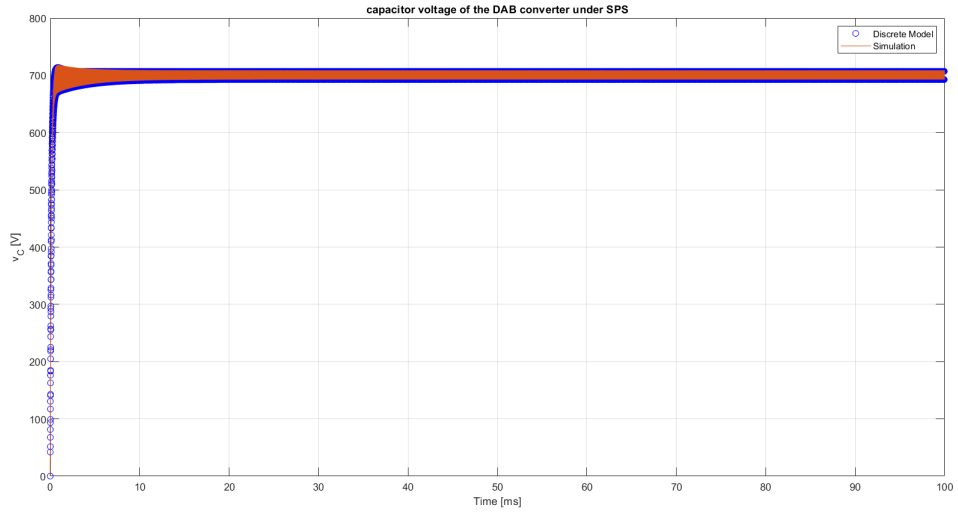

Figure 35: the capacitor voltage of the DAB converter under SPS

The data-points of the discrete model follow closely the waveform obtained by simulation, and the accuracy is highlighted in the following picture:

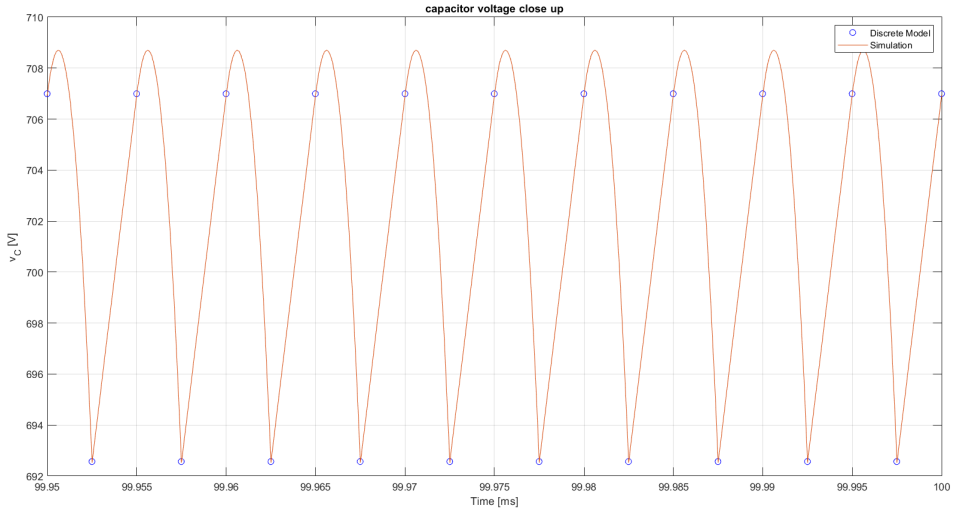

Figure 36: close caption of the waveform of the capacitor voltage under SPS

The data-point still follows the simulation waveform accurately, but the placement is not at the very top of the waveform. This is likely due to plotting distortion.

The model adjustments to suit the steady state operation of the DAB converter **under EPS** modulation are verified in a similar manner.

The comparison between the data-points of the discrete model and the simulation waveform of the steady state inductor current is shown in the figure below:

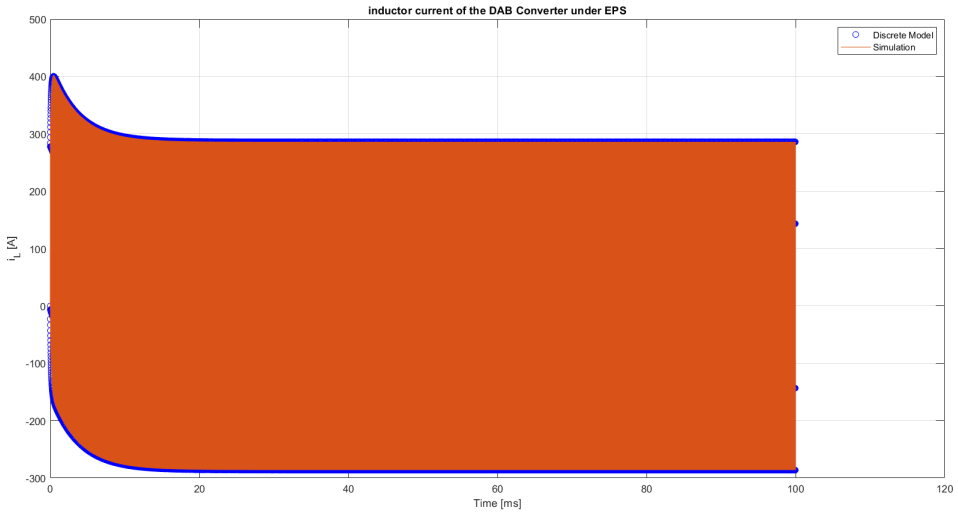

Figure 37: the inductor current of the DAB converter under EPS

The simulation and the model are seemingly overlapping. Upon taking a closer look, it

can indeed be noted that the accuracy is satisfactory:

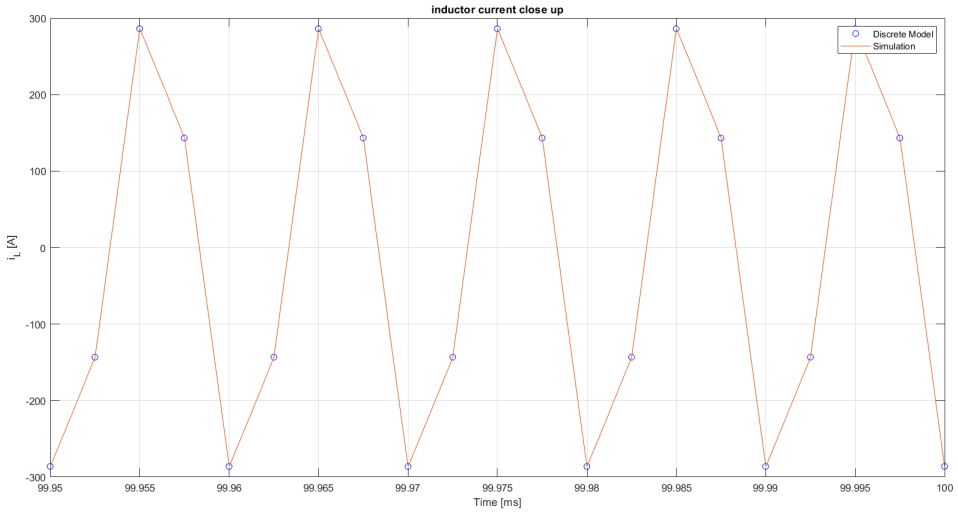

Figure 38: close caption of the inductor current under EPS

The voltage over the output capacitor of the DAB converter is depicted next, where the comparison between the data-points of the discrete model and the simulation can be studied:

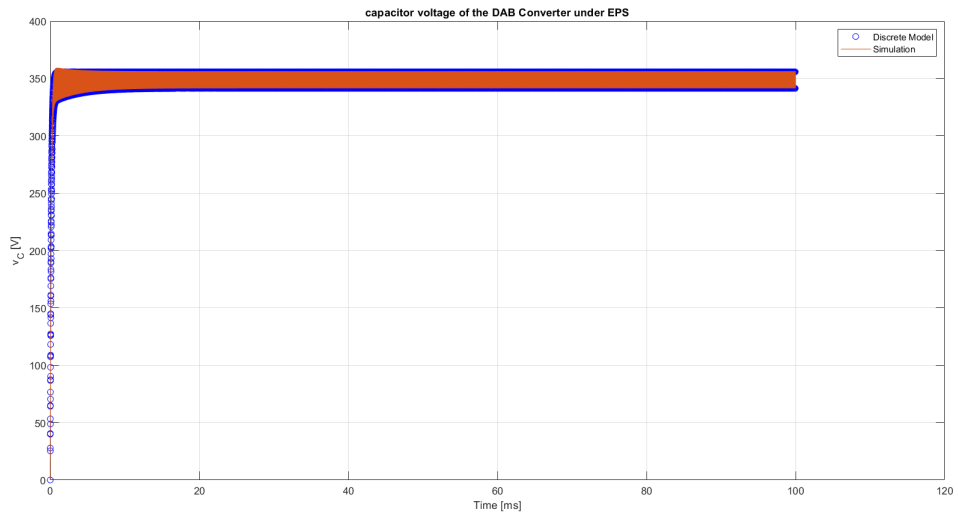

Figure 39: the capacitor voltage of the DAB converter under EPS

Once again, zooming in for a closer look reveals that the data points of discrete model are accurately overlapping with the waveform of the simulation:

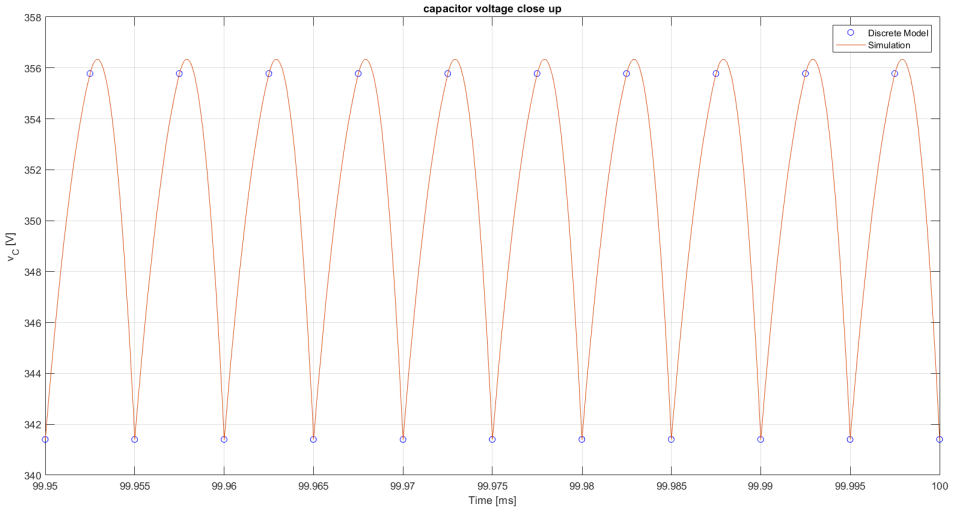

Figure 40: close caption of the capacitor voltage under EPS

4.3 Discussions

The goal of this thesis was to present and validate an optimal discrete time model of the DAB converter for operation under SPS and EPS, and it has been achieved. The derivation of a suitable model for the Buck converter has been carried out, both as a theoretical aid, and to build up intuition. Many of the concepts encountered in this paper apply to switched converters in general, and thus can be adapted to several device architectures.

It must however be stated that the initial ambitions of the author had to yield for the complexity of the subject. There were moments when the thesis was aiming at carrying out the derivation of the discrete model, followed by researching the best suited control method, subsequent implementation of the digital controller in the FPGA and testing the suitability of the control logic to the hardware itself. On the other hand, there were times when the focus was completely captured by one interesting theoretical concept. Studying the PhD dissertations of Cuk and Packard could easily fill an entire semester, just as well as the subject of nonlinearity and chaos could easily provide many years worth of food for the brain. The present work is therefore, like everything else in the field of engineering, a compromise. It is a compromise between what is desired and what can be delivered, considering the quality of the final product. The thorough and clear derivation of the discrete model had become the first priority of this thesis.

Writing this thesis has proved to be an intense learning activity. Truly understanding the

simple, yet complex nature of state space analysis has not been an easy task. While the traditional method of state space averaging, coupled with traditional control techniques can be, and are employed when dealing with switched power electronic devices, grasping the essence of why they are not the best suited tools was challenging. Building up the necessary skill-set to use the design software tools efficiently demanded time and effort. These tools have made possible the evolution of chaos as a science, and clearly proved that nonlinearity and fast dynamic behaviour should not be neglected and ignored, but instead visualised and planned for.

In conclusion, this paper is then a suitable foundation for researching of the optimal control methods, and implementing these control methods into the physical of the dual active bridge converter. It offers sufficient insight into the structure, characteristics and operation of the DAB converter. It introduces the reader to the relevant challenges that remain, the warning signs that frame the path ahead.

Bibliography

[1] M H Kheraluwala R W A A De Doncker M D Deepakraj. "A Three-Phase Soft Switched High-Power-Density dc/dc Converter for High-Power Applications". In: *IEEE Transactions of Industry Applications* 27.1 (1991), pp. 63–73.

[2] Jiawei Wang. "A Comparison between Si and SiC MOSFETs". In: *IOP Conference Series: Materials Science and Engineering*. IOP Conf. Ser.: Mater. Sci. Eng. 729 012005. 2020.

[3] F Roccaforte P Fiorenza G Greco R L Nigro F Giannazzo A Patti M Saggio. "Challenges for energy efficient wide band gap semiconductor power devices". In: *Phys. Status Solidi A* 211.9 (2014), pp. 2063–2071.

[4] F Wang Z Zhang E A Jones. *Characterization of Wide Bandgap Power Semiconductor Devices*. Stevenage: The Institution of Engineering and Technology, 2018.

[5] M A Bahmani. *Design and Optimization Considerations of Medium-Frequency Power Transformers in High-Power DC-DC Applications*. Division of Electric Power Engineering, Department of Energy and Environment, Chalmers University of Technology, Gothenburg, Sweden, 2016.

[6] Norbert Csongovai. *Specialisation project in TET4520*. Dec. 2021.

[7] Weixin Sun Biao Zhao Qingguang Yu. "Extended Phase Shift Control of Isolated Bidirectional DC-DC Converter for Power Distribution in Microgrid". In: *IEEE Transactions on Power Electronics* 27.11 (2012), pp. 4667–4680.

[8] J G Kassakian G C Verghese M E Elbuluk. "A General Approach to Sampled-Data Modeling for Power Electronic Circuits". In: *IEEE Transactions on Power Electronics* PE-1.2 (1986), pp. 76–89.

[9] D J Packard. *DISCRETE MODELING AND ANALYSIS OF SWITCHING REGULATORS*. California Institute of Technology, Pasadena California, 1976.

[10] E R Vilamitjana A El Aroudi E Alarcon. *Chaos in Switching Converters for Power Management*. Springer Science+Business Media New York, 2013. ISBN: 978-1-4614-2127-6.

[11] H Bai C Mi C Wang S Gargies. *The Dynamic Model and Hybrid Phase-Shift Control of a Dual-Active-Bridge Converter*. 2008.

[12] G Gkizas C Yfoulis C Amanatidis F Stergiopoulos D Giaouris C Ziogou S Voutetakis S Papadopoulou. "Digital state-feedback control of an interleaved DC–DC boost converter with bifurcation analysis". In: *Control Engineering Practice, Elsevier* 73 (2018), pp. 100–111.

[13] L.Shi W.Lei J.Huang Z.Li Y.Cui Y.Wang. "Full Discrete-Time Modeling and Stability Analysis of the Digital Controlled Dual Active Bridge Converter". In: *2016 IEEE 8th International Power Electronics and Motion Control Conference (IPEMC-ECCE Asia)*. IEEE. 2016, pp. 1–5.

[14] G D Demetriades. *ON SMALL-SIGNAL ANALYSIS AND CONTROL OF THE SINGLE-AND THE DUAL-ACTIVE BRIDGE TOPOLOGIES*. KTH Electrical Engineering, Stockholm, 2005. ISBN: 91-7283-966-X.

[15] J H B Deane D C Hamill. "Instability, Subharmonics, and Chaos in Power Electronic Systems". In: *IEEE Transactions on powere electronics* 5.3 (1990), pp. 260–268.

[16] D Pikulins. "Exploring Types of Instabilities in Switching Power Converters: the Complete Bifurcation Analysis". In: *ELEKTRONIKA IR ELEKTROTECHNIKA* 20.5 (2014), pp. 76–79.

[17] L Premalatha R Vanaja. "Implementation of FPGA based Digital Controller for Controlling Chaos in DC/DC converters". In: *Journal of Computer Science & Control Systems* 3.1 (2010), pp. 109–114.

[18] D Morcillo D Burbano F Angulo G Olivar. "Using Bifurcation Diagrams for Controlling Chaos". In: *Applied Non-Linear Dynamical Systems* (2014), pp. 77–84.

[19] Ogata Katsuhiko. *Discrte-Time Control Systems*. Prentice-Hall,Inc., 1995. ISBN: 0-13-328642-8.

[20] D Maksimovic D Costinett R Zane. *Discrete-Time Small-Signal Modeling of a 1 MHz Efficiency-Optimized Dual Active Bridge Converter With Varying Load*. 2012.

[21] L Shi W Lei Z Li J Huang Y Cui Y Wang. "Bilinear Discrete-Time Modeling and Stability Analysis of the Digitally Controlled Dual Active Bridge Converter". In: *IEEE Transactions on Power Electronics* 32.11 (2017), pp. 8787–8799.